SPATIAL ANCF/CRBF BEAM ELEMENTS

Shubhankar Kulkarni (skulka22@uic.edu)
Ahmed A. Shabana (shabana@uic.edu)

Department of Mechanical and Industrial Engineering
University of Illinois at Chicago
Chicago, IL 60607

ABSTRACT

In this paper, the *consistent rotation-based formulation* (CRBF) is used to develop new three-dimensional beam elements starting with the *absolute nodal coordinate formulation* (ANCF) kinematic description. While the proposed elements employ orientation parameters as nodal coordinates, independent rotation interpolation is avoided, leading to unique displacement and rotation fields. Furthermore, the proposed spatial ANCF/CRBF-based beam elements adhere to the non-commutative nature of the rotation parameters, allow for arbitrarily large three-dimensional rotation, and eliminate the need for using co-rotational or incremental solution procedures. Because the proposed elements have a general geometric description consistent with computational geometry methods, accurate definitions of the shear and bending deformations can be developed and evaluated, and curved structures and complex geometries can be systematically modeled. Three new spatial ANCF/CRBF beam elements, which use absolute positions and rotation parameters as nodal coordinates, are proposed. The time derivatives of the ANCF transverse position vector gradients at the nodes are expressed in terms of the time derivatives of rotation parameters using a nonlinear velocity transformation matrix. The velocity transformation leads to lower-dimensional elements that ensure the continuity of stresses and rotations at the element nodal points. The numerical results obtained from the proposed ANCF/CRBF elements are compared with the more general ANCF beam elements and with elements implemented in a commercial FE software.

Keywords: Consistent rotation-based formulation; absolute nodal coordinate formulation; flexible multibody system dynamics; large rotation vector formulation; shear deformation.

1. INTRODUCTION

Finite beam elements are widely used in the analysis of structural and mechanical system applications (Bathe, 1996; Belytschko et al., 2000; Bonet and Wood, 1997; Cook et al., 1989; Crisfield, 1991; Takahashi and Shimizu, 1999; Zienkkiewicz, 1977; Zienkkiewicz and Taylor, 2000). In mechanical system applications, in particular, accurate representation of the rotation and spinning motion is necessary for the development of robust solution algorithms (Roberson and Schwertassek, 1988; Wittenburg, 2007; Shabana, 2013). This investigation is focused on using a consistent rotation-based formulation (CRBF) to develop new finite beam elements for the large rotation and deformation analysis of flexible multibody system (MBS) applications. Several three-dimensional ANCF/CRBF beam elements are proposed and their performance is investigated. In this section, a brief literature survey of different beam element formulations is provided, with an emphasis on different approaches for representing the finite rotations in flexible MBS dynamics. The contributions of this study and the organization of the paper are also discussed.

1.1 Background

Different formulations have been used in the past to solve nonlinear flexible MBS dynamics problems. One of the main differences between these formulations is the way finite rotations are treated. The form of the displacement field of a formulation plays an important role in developing robust MBS solution algorithms which are based on non-incremental rotation procedures.

Because conventional structural finite elements such as beams, plates, and shells cannot accurately describe finite rotations non-incrementally (Bathe, 1996; Cook et al., 1989), the co-rotational formulation is often used for the solution of large rotation problems. In the co-rotational procedures, the global displacement field is decomposed into rigid body motion and deformation (Belytschko and Hsieh, 1973; Rankin and Brogan, 1986). The element forces are first defined in a

convected coordinate system and then transformed to a global system. This decomposition of the displacement field holds if the element deformation is not large in each time step to allow using the current element configuration, in which the equations are defined, as a valid reference configuration. Because it is also assumed that there is no large variation in the large reference motion in each time step, the time step size must remain small. It has been demonstrated in the literature that obtaining a solution for flexible MBS problems characterized by highly nonlinear inertia forces, motion constraints, and discontinuities can be difficult when co-rotational procedures are used (Campanelli et al., 2000). The non-incremental formulations, on the other hand, can accurately capture nonlinearities arising from the finite rotation (Pappalardo, 2015; Shabana, 2013).

The absolute nodal coordinate formulation (ANCF) was proposed for the analysis of flexible MBS applications characterized by large reference displacements and large elastic deformations. ANCF elements, which employ global position and gradient vectors as nodal coordinates, can be used with non-incremental procedures, define unique displacement and rotation fields, are related to computational geometry representations by linear mapping, and lead to a constant mass matrix and zero centrifugal and Coriolis inertia forces. Because of the use of the position vector gradients as nodal coordinates, ANCF elements, which do not employ an independent rotation field (Simo and Vu Quoc 1986; Ding et al., 2014; Shabana, 2010), have been used successfully in the study of many problems including MBS applications (Nachbagauer et al., 2011; Nachbagauer, 2013; Dmitrochenko and Mikkola, 2011; Gerstmayr and Irschik, 2008; Hu et al., 2014; Liu et al., 2011; Orzechowski, 2012; Orzechowski and Fraczek, 2012; Orzechowski and Fraczek, 2015; Tian et al., 2009; Tian et al., 2013; Patel et al., 2016; Kulkarni et al., 2017, Nicolsen et al., 2017).

The ANCF kinematic description can be used to develop a lower-order CRBF elements that employ finite orientation parameters as nodal coordinates without the need for using an independent interpolation for the rotation field, that is, the position vector $\mathbf{r}$ of the material points and the set of angles $\boldsymbol{\theta}$ that define the orientation of the cross section are not interpolated independently (Shabana, 2015). This approach is consistent with the theory of continuum mechanics in which the matrix of position vector gradients is defined using the position field (Bonet and Wood, 1997). The polar decomposition theorem can be used to define the orthogonal rotation and symmetric stretch tensors from the matrix of position vector gradients. Therefore, the position field of the material points can uniquely define the rotation and displacement of the material points. The ANCF/CRBF approach used in this paper also avoids independent interpolations of the position and rotation fields which lead to geometric redundancy issues and violate the aforementioned principle of continuum mechanics (Ding et al., 2014; Shabana, 2010). Furthermore, the ANCF/CRBF approach is different from the director-based approach proposed in some previous investigations which introduced rotation parameters with ANCF elements and employed independent interpolations of the positions and angles. Some of these studies reported instability problems with the solutions of longer simulation times (Gruber et al., 2013; Gerstmayr et al., 2017). Such instability problems are not observed, for the planar examples used in the literature, when using the ANCF/CRBF approach which is based on a nonlinear mapping between the rotation parameters and the position vector gradients.

Three-dimensional ANCF/CRBF elements can capture shear, bending, and torsion deformation modes and can be designed to eliminate high frequency modes associated with the deformation of the cross-section. To this end, a nonlinear velocity transformation is used to define the relationship between the time derivatives of the ANCF position vector gradients and the time

derivatives of the finite rotation parameters. This leads to a configuration-dependent nonlinear mass matrix and non-zero Coriolis and centrifugal forces. In recent investigations, planar CRBF beam and three-dimensional plate elements were proposed (Zheng and Shabana, 2017; Pappalardo et al., 2017). Therefore, the focus of this investigation will be on developing and examining the performance of new spatial ANCF/CRBF beam elements that can be used in MBS applications.

1.2 Scope and Contributions of this Investigation

In this paper, several new three-dimensional ANCF/CRBF beam elements consistent with geometry methods are developed. These elements can be used to model arbitrarily large displacements and initially curved geometries. Two of the elements developed in this study ensure the continuity of the rotation and stress fields. A third lower-order element, which ensures the continuity of the rotation field but does not ensure the continuity of the stress field, is also developed. Specifically, the main contributions of this paper can be summarized as follows:

(1) The three-dimensional kinematics of the beam element cross-section is first discussed in order to define the curvature, shear, and torsion measures. The curvature and torsion measures defined in the classical differential geometry by the Serret-Frenet equations are presented and used to shed light on the definitions obtained using the ANCF/CRBF rotational coordinates as well as the *material curvatures* used in the FE literature. The shear strain is defined using the dot product of two gradient vectors obtained by differentiation with respect to two independent parameters, and therefore, it cannot be determined from the Serret-Frenet equations which are based on the geometry of a curve defined by one parameter.

(2) A new spatial 18-degree-of-freedom ANCF/CRBF shear-deformable beam element is developed based on the kinematics of a fully parameterized ANCF element. This new element employs, as nodal coordinates, three position coordinates, three rotation parameters, and a

longitudinal position gradient vector. Using a nonlinear velocity transformation matrix, the time derivatives of the transverse position vector gradients are expressed in terms of the time derivatives of the rotational coordinates which are selected in this investigation to be Euler angles. This velocity transformation matrix, used to systematically define the mass matrix and elastic forces of the element, ensures the continuity of the rotation and stress fields.

(3) A second new ANCF/CRBF beam element which has 7 coordinates at each node is developed. The nodal coordinates of this element include three position coordinates, three rotation parameters, and an extensibility parameter in the longitudinal direction. In developing the kinematics of this element, the nodal position gradient vectors are assumed to remain orthogonal vectors, and therefore, this element does not experience shearing at the nodal points. The extensibility parameter used in the kinematic description of this element allows capturing axial stretch. This new element ensures the continuity of the rotation and stress fields.

(4) A third spatial CRBF beam element is developed based on the kinematics of a gradient deficient linear beam element. The new element has 12 degrees of freedom which consist of three positions and three rotational parameters at each node. While this element ensures the continuity of the rotation field, it does not ensure the continuity of the stress field.

(5) The proposed ANCF/CRBF and CRBF beam elements are implemented and their performance is evaluated using several static and dynamic problems. It is shown that the numerical results obtained from the proposed higher order ANCF/CRBF and linear CRBF elements compare well with the results obtained from the fully parameterized three-dimensional ANCF beam element and the beam element implemented in a commercial FE software. The fully parameterized ANCF beam locking problems are discussed and both the continuum and enhanced continuum mechanics approaches are used in order to evaluate the locking effect

(Nachbagauer et al., 2011; Nachbagauer et al., 2013; Nachbagauer, 2014; Patel and Shabana, 2018; Gerstmayr et al., 2008).

1.3 Limitations of the New Elements

The order of the ANCF/CRBF elements is lower than the order of the ANCF elements, and therefore, ANCF/CRBF elements cannot capture all the deformation modes captured by the more general ANCF elements. Because of the coordinate reduction, the mass matrix becomes a nonlinear function of the coordinates, and as a result, configuration-dependent. As the FE mesh size increases, the nonlinearity of the mass matrix can have a negative impact on the computational efficiency. Therefore, ANCF/CRBF elements can be less efficient for larger FE mesh as compared to ANCF elements which have a constant mass matrix and zero centrifugal and Coriolis forces. It is important, however, to point out that all other three-dimensional beam elements, except ANCF elements, have a nonlinear mass matrix in the case of large rotations when a consistent mass approach is used. Diagonal lumped mass matrices do not correctly represent the inertia of the flexible bodies that undergo finite rotations.

The choice of the orientation parameters for three-dimensional ANCF/CRBF elements can be an important issue. Different sets of orientation parameters can be selected; some of which may suffer from singularity problems (Roberson and Schwertassek, 1988; Wittenburg, 2007; Shabana, 2013). While Euler angles are used in this study to give obvious physical meaning to some of the deformation measures, other orientation parameters such as the four Euler parameters which do not suffer from the singularity problem can also be used. In the case of Euler parameters, however, the interpretation of some deformation modes of the beam can be less obvious and a nonlinear algebraic constraint equation that relates Euler parameters must be introduced at each node and must be satisfied at the position, velocity, and acceleration levels during the dynamic simulation.

1.4 Organization of the Paper

Section 2 of the paper discusses the beam cross-section kinematics as well as torsion, shear, and curvature measures. In Section 3, the formulation of the 18-degrees-of-freedom shear-deformable ANCF/CRBF element is presented, and the velocity transformation matrix is developed. Section 4 presents the formulation of the 14-degree-of-freedom three-dimensional ANCF/CRBF beam element which includes an extensibility parameter as a nodal coordinate. In Section 5, a linear 12-degree-of-freedom CRBF beam element formulation is presented. Because of the linear displacement field, the curvature within the element is zero, and classical differential geometry curvature definitions cannot be used with such a low order element. Section 6 shows the form of the equations of motion used, while in Section 7, numerical results of dynamic and static problems are reported to compare the elements, validate their solutions, and evaluate their performance. In Section 8, summary and conclusions of this investigation are presented.

2. KINEMATICS OF THE CROSS-SECTION

The ANCF/CRBF three-dimensional beam cross-section kinematics are discussed in this section in order to develop appropriate shear, torsion, and curvature measures. As previously mentioned, all the proposed ANCF/CRBF elements employ orientation parameters as nodal coordinates. These orientation parameters are systematically used to define orthogonal unit gradient vectors which define the cross-section of the beam. This definition is significant in the study of the kinematics and deformation modes of the ANCF/CRBF beam elements.

2.1 Curvature, Torsion, and Shear Measures

One of the important features of the CRBF elements is that orientation parameters can be systematically used to define the cross-section kinematics. The vector normal to the cross-section

of the beam can be selected to coincide with the tangent to the centerline in the case of Euler-Bernoulli beams. However, when a shear-deformable beam is considered, the tangent vector to the centerline is not, in general, parallel to the cross-section normal vector.

The ANCF/CRBF elements are based on the ANCF kinematic description. If the effect of all shear modes is neglected at the nodal points, the orientation parameters can be used to define the nodal position vector gradients $\mathbf{r}_x$, $\mathbf{r}_y$, and $\mathbf{r}_z$ as orthogonal unit vectors that represent the columns of an orthogonal matrix $\mathbf{A}(\boldsymbol{\theta}) = \begin{bmatrix} \mathbf{a}_1 & \mathbf{a}_2 & \mathbf{a}_3 \end{bmatrix}$, where $\boldsymbol{\theta}$ is the vector of orientation parameters, $\mathbf{r}$ is the global position vector, and x, y, and z are the element spatial coordinates. The global position vector $\mathbf{r}^c$ of an arbitrary point on the cross-section of the beam with respect to a point on the centerline at the intersection with the same cross-section can be defined as $\mathbf{r}^c = y\mathbf{r}_y + z\mathbf{r}_z$, demonstrating that an arbitrary vector drawn on the rigid and planar cross-section can be expressed as a linear combination of the transverse gradient vectors (Shabana and Yakoub, 2001). For example, in the case of the ANCF/CRBF three-dimensional beam elements introduced in Section 3, the transverse gradient vectors are interpolated linearly, that is, $\mathbf{r}_\alpha = (1-\xi)\mathbf{r}_\alpha^1 + \xi\mathbf{r}_\alpha^2$ where $\alpha = y, z$, $\xi = x/l$, l is the length of the beam, and superscripts 1 and 2 refer, respectively, to the first and second nodes of the element. As it is known, the interpolation of unit vectors does not lead to unit vectors, and the deviation in the magnitude from unity is maximum at the center of the element. This deviation remains relatively small as long as the relative rotation between $\mathbf{r}_\alpha^1$ and $\mathbf{r}_\alpha^2$ does not exceed 30° (Shabana, 2016). For the 30° relative angle using linear gradient interpolation for planar beams, the error is approximately 3.3%. Therefore, the norms of the gradient vectors $\mathbf{r}_y$ and $\mathbf{r}_z$ remain close to one.

When the Euler-Bernoulli beam assumptions are considered, the matrix $\mathbf{A}$ defining the three orthonormal position vector gradients at the nodes also define a local material frame which can be used to further define torsion and curvature measures that appear in the Serret-Frenet equations. The Serret-Frenet frame is a coordinate system which defines three vectors, a tangent vector $\mathbf{t}$, a normal vector $\mathbf{n}$ and a bi-normal vector $\mathbf{b}$ to the beam centerline (Kreyszig, 1991). When shear deformation is not considered in the ANCF/CRBF spatial beams, the first column of the matrix $\mathbf{A}$ defines the tangent to the centerline and the other two columns can be selected, without loss of generality, to be the normal and bi-normal vectors, implying that, $\mathbf{t} = \mathbf{a}_1 = \mathbf{r}_x$, $\mathbf{n} = \mathbf{a}_2$, and $\mathbf{b} = \mathbf{a}_3$. The skew-symmetric curvature-torsion matrix associated with this Serret-Frenet frame is $\tilde{\boldsymbol{\kappa}} = \mathbf{A}^T\mathbf{A}_s$, where the subscript s denotes differentiation with respect to the arc-length s (Kreyszig, 1991; Greenberg, 1998). Therefore, the skew-symmetric matrix $\tilde{\boldsymbol{\kappa}}$ can be written in terms of the curvature κ and torsion τ as,

$$\tilde{\boldsymbol{\kappa}} = \begin{bmatrix} 0 & -\kappa & 0 \\ \kappa & 0 & -\tau \\ 0 & \tau & 0 \end{bmatrix} \tag{1}$$

When the shear deformation is considered in the ANCF/CRBF beams, as will be discussed in this paper, the position vector gradient $\mathbf{r}_x$ along the longitudinal direction of the element remains the first column in the Serret-Frenet frame transformation matrix. The tangent vector can be defined as $\mathbf{t} = d\mathbf{r}/ds$, where $\mathbf{r}$ is the absolute position vector of a point on the element and ds is the arc-length of an infinitesimal segment of the centerline given by $ds = |\mathbf{r}_x|dx$. The normal vector can be defined as $\mathbf{n} = (d\mathbf{t}/ds)/(|d\mathbf{t}/ds|)$. The third vector which completes the Serret-Frenet orthogonal triad is the bi-normal vector $\mathbf{b}$ and is given by $\mathbf{b} = \mathbf{t} \times \mathbf{n}$. Thus, the orientation of this Serret-Frenet frame is given by the transformation matrix $\mathbf{A}^{sf} = [\mathbf{t} \quad \mathbf{n} \quad \mathbf{b}]$. The curvature and

torsion of the beam longitudinal fibers can be obtained from the Serret-Frenet formulae as described by Eq. 1. The exact geometric curvature is defined as $\kappa = \left|\mathbf{r}_{ss}\right| = \left|d\mathbf{t}/ds\right|$. The osculating plane is defined by the tangent and the normal vectors of the Serret-Frenet frame. Torsion is the rate at which a curve twists out of the osculating plane and is defined as $\tau = \left|d\mathbf{b}/ds\right|$.

The transverse position vector gradients can be expressed as orthogonal unit vectors in terms of nodal orientation parameters, hence a cross-section frame can be defined using three vectors as, $\mathbf{n}^c = \mathbf{r}_y = \mathbf{a}_2$, $\mathbf{b}^c = \mathbf{r}_z = \mathbf{a}_3$, and $\mathbf{t}^c = \mathbf{n}^c \times \mathbf{b}^c$. In case of shear deformation, the normal vector to the cross-section $\mathbf{t}^c$ is not, in general, parallel to the vector $\mathbf{t}$ tangent to the centerline. The relative rotations between these two vectors yield the in-plane and out-of-plane shear angles. The vector $\mathbf{t}$ can be considered as the axis of rotation and the rotation of the vector $\mathbf{t}^c$ about this vector can be expressed in terms of three independent rotation parameters as defined by Rodriguez formula (Roberson and Schwertassek, 1988; and Shabana, 2013). If the rotation of the cross-section defining torsion is excluded, two rotation parameters remain which define the two shear angles corresponding to the in-plane and out-of-plane shears, a description consistent with the general continuum mechanics approach; $\varepsilon_{12} = \left(\mathbf{r}_x \cdot \mathbf{r}_y\right)/2$ and $\varepsilon_{13} = \left(\mathbf{r}_x \cdot \mathbf{r}_z\right)/2$, where ε_{12} and ε_{13} are the continuum mechanics shear strains. In the case of small shear angles (infinitesimal rotations), the orientation of the cross-section frame with respect to the Serret-Frenet frame can be used to determine the in-plane shear angle γ_2 and out of plane shear angle γ_3 using the following matrix product:

$$\mathbf{A}^{sfT}\mathbf{A}^c = \begin{bmatrix} \mathbf{t}^T\mathbf{a}_1 & \mathbf{t}^T\mathbf{a}_2 & \mathbf{t}^T\mathbf{a}_3 \\ \mathbf{n}^T\mathbf{a}_1 & \mathbf{n}^T\mathbf{a}_2 & \mathbf{n}^T\mathbf{a}_3 \\ \mathbf{b}^T\mathbf{a}_1 & \mathbf{b}^T\mathbf{a}_2 & \mathbf{b}^T\mathbf{a}_3 \end{bmatrix} \approx \begin{bmatrix} 1 & -\gamma_3 & \gamma_2 \\ \gamma_3 & 1 & -\gamma_1 \\ -\gamma_2 & \gamma_1 & 1 \end{bmatrix} \tag{2}$$

Clearly, the angles γ_2 and γ_3 correspond, respectively, to the general continuum mechanics definition of the shear strains $\varepsilon_{12} = \left(\mathbf{r}_x \cdot \mathbf{r}_y\right)/2$ and $\varepsilon_{13} = \left(\mathbf{r}_x \cdot \mathbf{r}_z\right)/2$. If Euler angles are used to define the transformation matrix of the cross-section frame $\mathbf{A}^c$ and if the Serret-Frenet transformation matrix $\mathbf{A}^{sf}$ is defined in terms of the geometry of a space curve such as the element centerline, then the shear angle γ_2 and γ_3, and the torsion angle γ_1 can be expressed systematically in terms of Euler angles and the Serret-Frenet tangent, normal, and bi-normal vectors. In the case of large displacements and large deformations, more complex expressions are obtained, and in this case, the use of the continuum mechanics definitions of the shear strains to formulate the elastic forces is more straight-forward and is more accurate. It is also important to point out that the definition of the Serret-Frenet torsion τ in Eq. 1 cannot capture the rotation of the cross-section of a straight beam about its own axis since such a rotation does not change the position vector $\mathbf{r}$. Such a rotation, however, is captured by γ_1 of Eq. 2.

2.2 Material Curvature

For a spatial space curve, the curvature is defined by the Serret-Frenet formula as described in Eq. 1. According to the principles of continuum mechanics, bending and shear are two independent deformation modes and there exists no kinematic coupling between them, although they can be kinetically coupled. At an arbitrary point and along a certain direction, a beam can shear without bending and bend without shearing. Therefore, the use of a curvature definition, such as the *material curvature* definition, based on the cross-section orientation will produce non-zero bending energy in a non-uniform pure shear deformation mode (Zheng et al., 2018; Shabana and Patel, 2018). The material curvature is defined as $\tilde{\boldsymbol{\kappa}} = \mathbf{A}^{c^T}\mathbf{A}^c_s$, where the matrix $\mathbf{A}^c$ defines the orientation of the cross-section, and the subscript s denotes differentiation with respect to the arc

length of the beam longitudinal fiber. The total rotation of the cross-section includes the effect of bending, torsion, and shear as well as any finite rigid body rotation experienced by the beam. Therefore, when the curvature is defined from the cross-section orientation using the equation $\tilde{\boldsymbol{\kappa}} = \mathbf{A}^{c^T}\mathbf{A}_s^c$, the shear deformation is kinematically coupled with the bending deformation, which does not represent a correct shear definition and may lead to incorrect results in certain deformation modes. As demonstrated by Zheng et al. (2018), even in the simple case of planar motion, the equation $\tilde{\boldsymbol{\kappa}} = \mathbf{A}^{c^T}\mathbf{A}_s^c$ leads to $\tilde{\boldsymbol{\kappa}} = \mathbf{A}^{c^T}\left(d\mathbf{A}^c/ds\right) = \theta_s\tilde{\mathbf{A}}^{c^T}$, where θ is the angle that defines the orientation of the cross section in a planar motion, $\theta_s = \partial\theta/\partial s$, $\mathbf{A}^c = \left[\mathbf{a}_1 \quad \mathbf{a}_2\right]$, $\mathbf{a}_1 = \left[\cos\theta \quad \sin\theta\right]^T$, $\mathbf{a}_2 = \left[-\sin\theta \quad \cos\theta\right]^T$, $\tilde{\mathbf{A}} = \left[\mathbf{a}_{1s} \quad \mathbf{a}_{2s}\right]$, $\mathbf{a}_{1s} = \left[0 \quad -1\right]^T$ and $\mathbf{a}_{2s} = \left[0 \quad 1\right]^T$. As discussed by Zheng et al. (2018), the curvature is not the derivative of the angle that defines the orientation of the cross section; it is the derivative of the angle that defines the orientation of the unit tangent to the space curve which is the same as the magnitude of the curvature vector obtained by differentiating the unit tangent with respect to the arc length. One can also show that when ANCF elements are used, the material curvature converges to the correct curvature in the case of zero shear since the cross section remains in this special case along the normal to the centerline of the beam, which is the case of an Euler-Bernoulli beam.

3. ANCF/CRBF SHEAR-DEFORMABLE BEAM

This section describes the formulation of a new ANCF/CRBF 18-degree-of-freedom spatial element, referred to as *ANCF/CRBF18*. The vector of nodal coordinates for this element includes three position coordinates, three components of the longitudinal position gradient vector, and three rotational parameters. The time derivatives of the ANCF position vector gradients are expressed

in terms of the time derivatives of the orientation parameters using a velocity transformation that ensures that the transverse gradient vectors at the nodes remain orthogonal unit vectors. Shear deformation can be captured by this element since there is no orthogonality condition imposed on the longitudinal position vector gradient. This beam element can correctly describe rigid body motion and ensures continuity of the rotation and stress fields at the nodes.

3.1 Displacement Field

The formulation of the ANCF/CRBF18 beam element starts with the displacement field of the three-dimensional fully parameterized ANCF beam element (shown in Fig. 1), which can be written as $\mathbf{r}(\mathbf{x},t)=\mathbf{S}(\mathbf{x})\mathbf{e}(t)$, where $\mathbf{r}$ is the global position vector of an arbitrary point on the element, $\mathbf{S}$ is the element shape function matrix, $\mathbf{e}$ is the vector of nodal coordinates that includes absolute positions and position vector gradients, $\mathbf{x}=\begin{bmatrix}x & y & z\end{bmatrix}^T$ is the vector of element spatial coordinates, and t is the time (Yakoub and Shabana, 2001). This ANCF beam element is referred to in this paper as *ANCF24*. The interpolating polynomials used to define the displacement field are cubic in x and linear in y and z and are given by

$$\mathbf{r}=\begin{bmatrix} a_0+a_1x+a_2y+a_3z+a_4xy+a_5xz+a_6x^2+a_7x^3 \\ b_0+b_1x+b_2y+b_3z+b_4xy+b_5xz+b_6x^2+b_7x^3 \\ c_0+c_1x+c_2y+c_3z+c_4xy+c_5xz+c_6x^2+c_7x^3 \end{bmatrix} \tag{3}$$

where a_i, b_i and c_i, $i=0,1,2,...,7$ are the polynomial coefficients, and x, y, and z are the spatial coordinates defined in the beam coordinate system. The vector of nodal coordinates at a node k is given by $\mathbf{e}^k=\begin{bmatrix}\mathbf{r}^{k^T} & \mathbf{r}_x^{k^T} & \mathbf{r}_y^{k^T} & \mathbf{r}_z^{k^T}\end{bmatrix}^T$, where $\mathbf{r}$ is the global position vector and $\mathbf{r}_\beta=\partial\mathbf{r}/\partial\beta$, $\beta=x,y,z$ are the position vector gradients. The *ANCF24* element has 24 nodal

coordinates which can be written as $\mathbf{e} = \left[\mathbf{e}^{1^T} \quad \mathbf{e}^{2^T} \right]^T$, where the superscripts refer to the two nodes of the element. The shape function matrix $\mathbf{S}$ for the element is defined as

$$\mathbf{S} = \left[S_1\mathbf{I} \quad S_2\mathbf{I} \quad S_3\mathbf{I} \quad S_4\mathbf{I} \quad S_5\mathbf{I} \quad S_6\mathbf{I} \quad S_7\mathbf{I} \quad S_8\mathbf{I} \right] \tag{4}$$

where $\mathbf{I}$ is the 3×3 identity matrix, and the shape functions $S_k, k = 1, 2, \ldots, 8$, are given by

$$\left.\begin{aligned} &S_1 = 1 - 3\xi^2 + 2\xi^3, \quad S_2 = l\left(\xi - 2\xi^2 + \xi^3\right), \\ &S_3 = l\left(\eta - \xi\eta\right), \quad S_4 = l\left(\zeta - \xi\zeta\right), \\ &S_5 = 3\xi^2 - 2\xi^3, \; S_6 = l\left(-\xi^2 + \xi^3\right), \; S_7 = l\xi\eta, \; S_8 = l\xi\zeta \end{aligned}\right\} \tag{5}$$

where $\xi = x/l$, $\eta = y/l$, and $\zeta = z/l$, and l is the element length. The ranges for x, y and z are $x \in [0,\ l]$, $y \in \left[-w/2,\ w/2\right]$, and $z \in \left[-h/2,\ h/2\right]$, where w and h are the width and the height of the element, respectively. Other types of cross-section can be conveniently used with the proposed elements as well (Orzechowski, 2012).

3.2 Characterization of the Finite Rotation

While the position equations are, in general, nonlinear in the orientation parameters, the velocity equations are linear functions in the time derivatives of these parameters. This fact is used in this section to develop the equations of the ANCF/CRBF18 beam element without violating the basic principles of continuum mechanics in which position coordinates are interpolated only. To this end, Euler angles, selected in this investigation as the orientation parameters, are used to develop the relationship between the time derivatives of the position vector gradients and the angular velocity vector. For a fully parameterized ANCF beam element, the matrix of position vector gradients $\mathbf{J}$ can be written as $\mathbf{J} = \left[\mathbf{r}_x \quad \mathbf{r}_y \quad \mathbf{r}_z \right]$. In the case of the ANCF/CRBF18 element, the transverse position vector gradients are assumed orthogonal unit vectors at the nodes. Thus, one can use the orthogonal matrix $\mathbf{A}(\boldsymbol{\theta}) = \left[\mathbf{a}_1 \quad \mathbf{a}_2 \quad \mathbf{a}_3 \right]$ to obtain expressions for transverse position

vector gradients, where $\boldsymbol{\theta}$ are the rotation parameters. It follows that $\dot{\mathbf{J}} = \begin{bmatrix} \dot{\mathbf{r}}_x & \dot{\mathbf{r}}_y & \dot{\mathbf{r}}_z \end{bmatrix} = \begin{bmatrix} \dot{\mathbf{r}}_x & \tilde{\boldsymbol{\omega}}\mathbf{a}_2 & \tilde{\boldsymbol{\omega}}\mathbf{a}_3 \end{bmatrix}$, where $\tilde{\boldsymbol{\omega}} = \dot{\mathbf{A}}\mathbf{A}^T$ is a skew symmetric matrix associated with the angular velocity vector $\boldsymbol{\omega} = \begin{bmatrix} \omega_1 & \omega_2 & \omega_3 \end{bmatrix}^T$. Because the angular velocity vector $\boldsymbol{\omega}$ can always be written as $\boldsymbol{\omega} = \mathbf{G}\dot{\boldsymbol{\theta}}$, where $\mathbf{G}$ is a matrix that depends on the orientation parameters; the relationship between the time derivatives of the position vector gradients and the orientation parameters can be written as

$$\dot{\mathbf{J}} = \begin{bmatrix} \dot{\mathbf{r}}_x & \dot{\mathbf{r}}_y & \dot{\mathbf{r}}_z \end{bmatrix} = \begin{bmatrix} \dot{\mathbf{r}}_x & -\tilde{\mathbf{a}}_2\boldsymbol{\omega} & -\tilde{\mathbf{a}}_3\boldsymbol{\omega} \end{bmatrix} = \begin{bmatrix} \dot{\mathbf{r}}_x & -\tilde{\mathbf{a}}_2\mathbf{G}\dot{\boldsymbol{\theta}} & -\tilde{\mathbf{a}}_3\mathbf{G}\dot{\boldsymbol{\theta}} \end{bmatrix} \tag{6}$$

where $\tilde{\mathbf{a}}_2$ and $\tilde{\mathbf{a}}_3$ are the skew symmetric matrices associated with the vectors $\mathbf{a}_2$ and $\mathbf{a}_3$, respectively. In this case, no condition is imposed on the longitudinal position vector gradient $\mathbf{r}_x$ in order to allow for capturing the shear deformation. Because of the orthogonality of $\mathbf{r}_y$ and $\mathbf{r}_z$, the transverse normal strain components ε_{22} and ε_{33}, and the shear strain ε_{23} remain zero, ensuring that the cross-section of the beam does not deform and remains planar and rigid at the nodes .

Because in the case of Euler angles, $\dot{\mathbf{G}}\dot{\boldsymbol{\theta}} \neq \mathbf{0}$ in general, the second time derivatives of the position vector gradients can be written as

$$\left.\begin{aligned} \ddot{\mathbf{r}}_y &= -\left(\mathbf{a}_2 \times \mathbf{G}\ddot{\boldsymbol{\theta}} + \mathbf{a}_2 \times \dot{\mathbf{G}}\dot{\boldsymbol{\theta}} + \left(\boldsymbol{\omega} \times \mathbf{a}_2\right) \times \mathbf{G}\dot{\boldsymbol{\theta}}\right) \\ \ddot{\mathbf{r}}_z &= -\left(\mathbf{a}_3 \times \mathbf{G}\ddot{\boldsymbol{\theta}} + \mathbf{a}_3 \times \dot{\mathbf{G}}\dot{\boldsymbol{\theta}} + \left(\boldsymbol{\omega} \times \mathbf{a}_3\right) \times \mathbf{G}\dot{\boldsymbol{\theta}}\right) \end{aligned}\right\} \tag{7}$$

In this investigation, the orthogonal transformation matrix $\mathbf{A}$ is obtained by performing successive rotations ϕ, θ, and ψ about the axes X, Y, and Z, respectively, leading to

$$\begin{aligned} \mathbf{A} &= \begin{bmatrix} \mathbf{a}_1 & \mathbf{a}_2 & \mathbf{a}_2 \end{bmatrix} \\ &= \begin{bmatrix} \cos\theta\cos\psi & -\cos\theta\sin\psi & \sin\theta \\ \sin\phi\sin\theta\cos\psi + \cos\phi\sin\psi & \cos\phi\cos\psi - \sin\phi\sin\theta\sin\psi & -\sin\phi\cos\theta \\ -\cos\phi\sin\theta\cos\psi + \sin\phi\sin\psi & \sin\phi\cos\psi + \cos\phi\sin\theta\sin\psi & \cos\phi\cos\theta \end{bmatrix} \end{aligned} \tag{8}$$

In this case, one has

$$\mathbf{G}=\begin{bmatrix}1 & 0 & \sin\theta\\ 0 & \cos\phi & -\sin\phi\cos\theta\\ 0 & \sin\phi & \cos\phi\cos\theta\end{bmatrix} \tag{9}$$

The matrix $\mathbf{G}$ becomes singular when $\theta=(2n+1)\pi/2$, where n is an integer. As previously mentioned, Euler parameters can be used to avoid the singularity at the expense of introducing an algebraic constraint equation at each node. The use of angles is also advantageous because, in the case of infinitesimal rotations, Euler angles can be related to the shear and torsion.

3.3 Velocity Transformation

The kinematic equations developed in this section can be systematically used to obtain the velocity transformation matrix that defines the relationship between ANCF coordinates and ANCF/CRBF coordinates at a node as

$$\begin{bmatrix}\dot{\mathbf{r}}\\ \dot{\mathbf{r}}_x\\ \dot{\mathbf{r}}_y\\ \dot{\mathbf{r}}_z\end{bmatrix}=\begin{bmatrix}\mathbf{I} & \mathbf{0} & \mathbf{0}\\ \mathbf{0} & \mathbf{I} & \mathbf{0}\\ \mathbf{0} & \mathbf{0} & -\tilde{\mathbf{a}}_2\mathbf{G}\\ \mathbf{0} & \mathbf{0} & -\tilde{\mathbf{a}}_3\mathbf{G}\end{bmatrix}\begin{bmatrix}\dot{\mathbf{r}}\\ \dot{\mathbf{r}}_x\\ \dot{\boldsymbol{\theta}}\end{bmatrix} \tag{10}$$

where $\mathbf{I}$ is the 3×3 identity matrix. The acceleration-level equations can be written as

$$\begin{bmatrix}\ddot{\mathbf{r}}\\ \ddot{\mathbf{r}}_x\\ \ddot{\mathbf{r}}_y\\ \ddot{\mathbf{r}}_z\end{bmatrix}=\begin{bmatrix}\mathbf{I} & \mathbf{0} & \mathbf{0}\\ \mathbf{0} & \mathbf{I} & \mathbf{0}\\ \mathbf{0} & \mathbf{0} & -\tilde{\mathbf{a}}_2\mathbf{G}\\ \mathbf{0} & \mathbf{0} & -\tilde{\mathbf{a}}_3\mathbf{G}\end{bmatrix}\begin{bmatrix}\ddot{\mathbf{r}}\\ \ddot{\mathbf{r}}_x\\ \ddot{\boldsymbol{\theta}}\end{bmatrix}+\begin{bmatrix}\mathbf{0}\\ \mathbf{0}\\ \boldsymbol{\omega}\times(\boldsymbol{\omega}\times\mathbf{a}_2)-\mathbf{a}_2\times\dot{\mathbf{G}}\dot{\boldsymbol{\theta}}\\ \boldsymbol{\omega}\times(\boldsymbol{\omega}\times\mathbf{a}_3)-\mathbf{a}_3\times\dot{\mathbf{G}}\dot{\boldsymbol{\theta}}\end{bmatrix} \tag{11}$$

This equation can be written for a node k as

$$\ddot{\mathbf{e}}^k=\mathbf{B}^k\ddot{\mathbf{p}}^k+\boldsymbol{\gamma}^k \tag{12}$$

where $k=1,2,\ldots,n$, n is the number of nodes, and

$$\mathbf{e}^k = \begin{bmatrix} \mathbf{r}^k \\ \mathbf{r}_x^k \\ \mathbf{r}_y^k \\ \mathbf{r}_z^k \end{bmatrix}, \ \mathbf{B}^k = \begin{bmatrix} \mathbf{I} & \mathbf{0} & \mathbf{0} \\ \mathbf{0} & \mathbf{I} & \mathbf{0} \\ \mathbf{0} & \mathbf{0} & -\tilde{\mathbf{a}}_2^k \mathbf{G}^k \\ \mathbf{0} & \mathbf{0} & -\tilde{\mathbf{a}}_3^k \mathbf{G}^k \end{bmatrix}, \ \mathbf{p}^k = \begin{bmatrix} \mathbf{r}^k \\ \mathbf{r}_x^k \\ \boldsymbol{\theta}^k \end{bmatrix}, \ \boldsymbol{\gamma}^k = \begin{bmatrix} \mathbf{0} \\ \mathbf{0} \\ \boldsymbol{\omega}^k \times \left(\boldsymbol{\omega}^k \times \mathbf{a}_2^k \right) - \mathbf{a}_2^k \times \dot{\mathbf{G}}^k \dot{\boldsymbol{\theta}}^k \\ \boldsymbol{\omega}^k \times \left(\boldsymbol{\omega}^k \times \mathbf{a}_3^k \right) - \mathbf{a}_3^k \times \dot{\mathbf{G}}^k \dot{\boldsymbol{\theta}}^k \end{bmatrix} \tag{13}$$

In Eq. 13, $\mathbf{e}^k$ is the vector of ANCF nodal coordinates at node k, $\mathbf{B}^k$ is the velocity transformation matrix associated with node k, $\mathbf{p}^k$ is the vector of nodal coordinates of the ANCF/CRBF element at node k, and $\boldsymbol{\gamma}^k$ is the vector which absorbs terms that are quadratic in the velocities. Using Eq. 12 and the element connectivity conditions, one has the ANCF/CRBF mesh equations

$$\ddot{\mathbf{e}} = \mathbf{B}\ddot{\mathbf{p}} + \boldsymbol{\gamma} \tag{14}$$

where

$$\mathbf{e} = \begin{bmatrix} \mathbf{e}^1 \\ \mathbf{e}^2 \\ \vdots \\ \mathbf{e}^n \end{bmatrix}, \quad \mathbf{B} = \begin{bmatrix} \mathbf{B}^1 & \mathbf{0} & \mathbf{0} & \mathbf{0} \\ \mathbf{0} & \mathbf{B}^2 & \mathbf{0} & \mathbf{0} \\ \vdots & \vdots & \ddots & \vdots \\ \mathbf{0} & \mathbf{0} & \mathbf{0} & \mathbf{B}^n \end{bmatrix}, \quad \mathbf{p} = \begin{bmatrix} \mathbf{p}^1 \\ \mathbf{p}^2 \\ \vdots \\ \mathbf{p}^n \end{bmatrix}, \quad \boldsymbol{\gamma} = \begin{bmatrix} \boldsymbol{\gamma}^1 \\ \boldsymbol{\gamma}^2 \\ \vdots \\ \boldsymbol{\gamma}^n \end{bmatrix} \tag{15}$$

The kinematic equations developed in this section will be used in a later section of this paper to define the governing equations of motion of the ANCF/CRBF mesh. Similar equations can be developed using other sets of orientation parameters by only changing the form of the two matrices $\mathbf{A}$ and $\mathbf{G}$.

4. ANCF/CRBF BEAM WITH EXTENSIBILITY

The three-dimensional 14-degree-of-freedom ANCF/CRBF beam element, referred to as *ANCF/CRBF14*, employs as nodal coordinates absolute positions, orientation parameters, and an extensibility parameter along the longitudinal direction of the beam at each node. The kinematic description of this element is also based on the displacement field of the *ANCF24* element. For the

ANCF/CRBF14 element, all the gradient vectors, $\mathbf{r}_x$, $\mathbf{r}_y$, and $\mathbf{r}_z$ are assumed to be orthogonal vectors at the nodes. Therefore, the cross-section does not deform and shear deformation is eliminated at the nodal points, leading to Euler-Bernoulli beam assumptions. An extensibility parameter α is used in the axial direction of the beam to allow for capturing stretch. In this case, the longitudinal gradient vector can be written as $\mathbf{r}_x = \alpha \mathbf{a}_1$, which upon differentiation leads to $\dot{\mathbf{r}}_x = \alpha \dot{\mathbf{a}}_1 + \dot{\alpha}\mathbf{a}_1 = \alpha\left(\boldsymbol{\omega} \times \mathbf{a}_1\right) + \dot{\alpha}\mathbf{a}_1$. Since $\boldsymbol{\omega} \times \mathbf{a}_1 = -\mathbf{a}_1 \times \boldsymbol{\omega} = -\tilde{\mathbf{a}}_1 \mathbf{G}\dot{\boldsymbol{\theta}}$, one has $\dot{\mathbf{r}}_x = -\alpha\tilde{\mathbf{a}}_1\mathbf{G}\dot{\boldsymbol{\theta}} + \dot{\alpha}\mathbf{a}_1$. Using this equation and following the procedure described in the preceding section, one has

$$\dot{\mathbf{J}} = \begin{bmatrix} \dot{\mathbf{r}}_x & \dot{\mathbf{r}}_y & \dot{\mathbf{r}}_z \end{bmatrix} = \begin{bmatrix} (-\alpha\tilde{\mathbf{a}}_1\mathbf{G}\dot{\boldsymbol{\theta}} + \mathbf{a}_1\dot{\alpha}) & -\tilde{\mathbf{a}}_2\mathbf{G}\dot{\boldsymbol{\theta}} & -\tilde{\mathbf{a}}_3\mathbf{G}\dot{\boldsymbol{\theta}} \end{bmatrix} \tag{16}$$

The second time derivatives of the gradient vectors can be written as

$$\left.\begin{aligned} \ddot{\mathbf{r}}_x &= -\alpha\left(\mathbf{a}_1 \times \mathbf{G}\ddot{\boldsymbol{\theta}}\right) + \mathbf{a}_1\ddot{\alpha} + \alpha\left(\boldsymbol{\omega} \times \left(\boldsymbol{\omega} \times \mathbf{a}_1\right)\right) + 2\dot{\alpha}\left(\boldsymbol{\omega} \times \mathbf{a}_1\right) - \alpha\left(\mathbf{a}_1 \times \dot{\mathbf{G}}\dot{\boldsymbol{\theta}}\right) \\ \ddot{\mathbf{r}}_y &= -\mathbf{a}_2 \times \mathbf{G}\ddot{\boldsymbol{\theta}} + \boldsymbol{\omega} \times \left(\boldsymbol{\omega} \times \mathbf{a}_2\right) - \mathbf{a}_2 \times \dot{\mathbf{G}}\dot{\boldsymbol{\theta}} \\ \ddot{\mathbf{r}}_z &= -\mathbf{a}_3 \times \mathbf{G}\ddot{\boldsymbol{\theta}} + \boldsymbol{\omega} \times \left(\boldsymbol{\omega} \times \mathbf{a}_3\right) - \mathbf{a}_3 \times \dot{\mathbf{G}}\dot{\boldsymbol{\theta}} \end{aligned}\right\} \tag{17}$$

The velocity relationship for the *ANCF/CRBF14* element is

$$\begin{bmatrix} \dot{\mathbf{r}} \\ \dot{\mathbf{r}}_x \\ \dot{\mathbf{r}}_y \\ \dot{\mathbf{r}}_z \end{bmatrix} = \begin{bmatrix} \mathbf{I} & \mathbf{0} & \mathbf{0} \\ \mathbf{0} & -\alpha\tilde{\mathbf{a}}_1\mathbf{G} & \mathbf{a}_1 \\ \mathbf{0} & -\tilde{\mathbf{a}}_2\mathbf{G} & \mathbf{0} \\ \mathbf{0} & -\tilde{\mathbf{a}}_3\mathbf{G} & \mathbf{0} \end{bmatrix} \begin{bmatrix} \dot{\mathbf{r}} \\ \dot{\boldsymbol{\theta}} \\ \dot{\alpha} \end{bmatrix} \tag{18}$$

For the *ANCF/CRBF14* element, the matrices of node k that appear in Eq. 12 are

$$\left.\begin{aligned}
\mathbf{e}^k &= \begin{bmatrix} \mathbf{r}^k \\ \mathbf{r}_x^k \\ \mathbf{r}_y^k \\ \mathbf{r}_z^k \end{bmatrix},\ \mathbf{B}^k = \begin{bmatrix} \mathbf{I} & \mathbf{0} & \mathbf{0} \\ \mathbf{0} & -\alpha^k \tilde{\mathbf{a}}_1^k \mathbf{G}^k & \mathbf{a}_1^k \\ \mathbf{0} & -\tilde{\mathbf{a}}_2^k \mathbf{G}^k & \mathbf{0} \\ \mathbf{0} & -\tilde{\mathbf{a}}_3^k \mathbf{G}^k & \mathbf{0} \end{bmatrix},\ \mathbf{p}^k = \begin{bmatrix} \mathbf{r}^k \\ \boldsymbol{\theta}^k \\ \alpha^k \end{bmatrix}, \\
\boldsymbol{\gamma}^k &= \begin{bmatrix} \mathbf{0} \\ \alpha^k \left(\boldsymbol{\omega}^k \times \left(\boldsymbol{\omega}^k \times \mathbf{a}_1^k \right) \right) + 2\dot{\alpha}^k \left(\boldsymbol{\omega}^k \times \mathbf{a}_1^k \right) - \alpha^k \left(\mathbf{a}_1^k \times \dot{\mathbf{G}}^k \dot{\boldsymbol{\theta}}^k \right) \\ \boldsymbol{\omega}^k \times \left(\boldsymbol{\omega}^k \times \mathbf{a}_2^k \right) - \mathbf{a}_2^k \times \dot{\mathbf{G}}^k \dot{\boldsymbol{\theta}}^k \\ \boldsymbol{\omega}^k \times \left(\boldsymbol{\omega}^k \times \mathbf{a}_3^k \right) - \mathbf{a}_3^k \times \dot{\mathbf{G}}^k \dot{\boldsymbol{\theta}}^k \end{bmatrix}
\end{aligned}\right\} \tag{19}$$

Using these matrices, an equation similar to Eq. 14 can be developed for this element.

5. LOWER ORDER LINEAR CRBF BEAM ELEMENT

The element developed in this section, referred to as *CRBF12*, has six coordinates per node which include three positions and three rotation parameters. The *CRBF12* element is derived from a lower order 18-degree-of-freedom linear element, referred to as *LINBEAM18*, which employs positions and only transverse position vector gradients as nodal coordinates and can be considered as the three-dimensional version of the planar element presented in the literature (Matikainen et al., 2010). The *LINBEAM18* element does not ensure continuity of the longitudinal position vector gradient $\mathbf{r}_x$. The interpolation polynomials chosen for the *LINBEAM18* element are

$$\mathbf{r} = \begin{bmatrix} a_0 + a_1 x + a_2 y + a_3 z + a_4 xy + a_5 xz \\ b_0 + b_1 x + b_2 y + b_3 z + b_4 xy + b_5 xz \\ c_0 + c_1 x + c_2 y + c_3 z + c_4 xy + c_5 xz \end{bmatrix} \tag{20}$$

where a_i, b_i, and c_i, $i = 0,1,2,...,5$ are the polynomial coefficients. Using these polynomials, the element displacement field can be written as $\mathbf{r}(\mathbf{x},\mathrm{t}) = \mathbf{S}(\mathbf{x})\mathbf{e}(\mathrm{t})$, where $\mathbf{e} = \begin{bmatrix} \mathbf{e}^{1^T} & \mathbf{e}^{2^T} \end{bmatrix}^T$ is the vector of nodal coordinate, $\mathbf{e}^k = \begin{bmatrix} \mathbf{r}^{k^T} & \mathbf{r}_y^{k^T} & \mathbf{r}_z^{k^T} \end{bmatrix}^T, k = 1,2$,

$$\mathbf{S} = \begin{bmatrix} S_1\mathbf{I} & S_2\mathbf{I} & S_3\mathbf{I} & S_4\mathbf{I} & S_5\mathbf{I} & S_6\mathbf{I} \end{bmatrix}, \tag{21}$$

$\mathbf{I}$ is the 3×3 identity matrix, and the shape functions are given by

$$\left.\begin{aligned} S_1 &= 1-\xi,\ S_2 = l\left(\eta-\xi\eta\right),\ S_3 = l\left(\zeta-\xi\zeta\right),\\ S_4 &= \xi,\ S_5 = l\xi\eta,\ S_6 = l\xi\zeta \end{aligned}\right\} \tag{22}$$

Following a procedure similar to the one previously used in this paper, one can write

$$\begin{bmatrix} \dot{\mathbf{r}} \\ \dot{\mathbf{r}}_y \\ \dot{\mathbf{r}}_z \end{bmatrix} = \begin{bmatrix} \mathbf{I} & \mathbf{0} \\ \mathbf{0} & -\tilde{\mathbf{a}}_2\mathbf{G} \\ \mathbf{0} & -\tilde{\mathbf{a}}_3\mathbf{G} \end{bmatrix} \begin{bmatrix} \dot{\mathbf{r}} \\ \dot{\boldsymbol{\theta}} \end{bmatrix} \tag{23}$$

The *CRBF12* element vectors and matrices at node k used in Eq. 12 are

$$\left.\begin{aligned} \mathbf{e}^k &= \begin{bmatrix} \mathbf{r}^k \\ \mathbf{r}_y^k \\ \mathbf{r}_z^k \end{bmatrix},\ \mathbf{B}^k = \begin{bmatrix} \mathbf{I} & \mathbf{0} \\ \mathbf{0} & -\tilde{\mathbf{a}}_2^k\mathbf{G}^k \\ \mathbf{0} & -\tilde{\mathbf{a}}_3^k\mathbf{G}^k \end{bmatrix},\\ \mathbf{p}^k &= \begin{bmatrix} \mathbf{r}^k \\ \boldsymbol{\theta}^k \end{bmatrix},\ \boldsymbol{\gamma}^k = \begin{bmatrix} \mathbf{0} \\ \boldsymbol{\omega}^k\times\left(\boldsymbol{\omega}^k\times\mathbf{a}_2^k\right)-\mathbf{a}_2^k\times\dot{\mathbf{G}}^k\dot{\boldsymbol{\theta}}^k \\ \boldsymbol{\omega}^k\times\left(\boldsymbol{\omega}^k\times\mathbf{a}_3^k\right)-\mathbf{a}_3^k\times\dot{\mathbf{G}}^k\dot{\boldsymbol{\theta}}^k \end{bmatrix} \end{aligned}\right\} \tag{24}$$

The form of the acceleration equations of the *CRBF12* mesh is the same as given by Eq. 14.

6. ELEMENT EQUATIONS OF MOTION

The element velocity transformation matrix can be used to develop the CRBF equations of motion at the element level from the ANCF element equations of motion. These equations of motion can be assembled to obtain the mesh equations of motion. Another alternate, yet equivalent, approach described in this section is to use the assembled ANCF element equations and the mesh velocity transformation matrix (Eq. 14) to obtain directly the assembled CRBF equations. The assembled ANCF system equations of motion can be written as $\mathbf{M}\ddot{\mathbf{e}} = \mathbf{Q}$, where $\ddot{\mathbf{e}}$ is the ANCF mesh nodal

acceleration vector, $\mathbf{M}$ is the constant and symmetric mesh mass matrix, and $\mathbf{Q}$ is the total vector of the generalized nodal forces. Substituting Eq. 14 into the ANCF equation of motion and pre-multiplying both sides of the equation $\mathbf{M}\ddot{\mathbf{e}} = \mathbf{Q}$ by the transpose of the system velocity transformation matrix, the equations of motion for the ANCF/CRBF and the CRBF elements are obtained as $\left(\mathbf{B}^T\mathbf{M}\mathbf{B}\right)\ddot{\mathbf{p}} = \mathbf{B}^T\left(\mathbf{Q} - \mathbf{M}\boldsymbol{\gamma}\right)$, which can be further written as $\bar{\mathbf{M}}\ddot{\mathbf{p}} = \bar{\mathbf{Q}}$, where $\bar{\mathbf{M}} = \mathbf{B}^T\mathbf{M}\mathbf{B}$ is the mass matrix which is configuration-dependent and nonlinear in the CRBF nodal coordinates, $\bar{\mathbf{Q}} = \mathbf{B}^T\left(\mathbf{Q} - \mathbf{M}\boldsymbol{\gamma}\right)$ is the generalized nodal force vector associated with CRBF elements, and $\ddot{\mathbf{p}}$ is the vector of CRBF nodal accelerations. The equations of motion $\bar{\mathbf{M}}\ddot{\mathbf{p}} = \bar{\mathbf{Q}}$ can be solved using direct numerical integration methods.

Because the fully parametrized ANCF beam element, *ANCF24*, suffers from locking problems, it can produce inaccurate results in some problems (Nachbagauer et al., 2011; Nachbagauer et al., 2013; Nachbagauer, 2014; Patel and Shabana, 2017). Several locking alleviation techniques have been applied to obtain improved solutions. In this investigation, the general continuum mechanics and enhanced continuum mechanics techniques are used to evaluate the element elastic forces (Nachbagauer et al., 2013). With the general continuum mechanics approach, the strain energy of a beam element with rectangular cross-section can be written as

$$U_G = \frac{1}{2}\int_{-W/2}^{W/2}\int_{-H/2}^{H/2}\int_{0}^{L}\boldsymbol{\varepsilon}^T\boldsymbol{\sigma}_{P2}J_0\,dxdydz \tag{25}$$

where $\boldsymbol{\varepsilon} = \begin{bmatrix}\varepsilon_{xx} & \varepsilon_{yy} & \varepsilon_{zz} & 2\varepsilon_{xy} & 2\varepsilon_{xz} & 2\varepsilon_{yz}\end{bmatrix}^T$ and $\boldsymbol{\sigma}_{P2}$ are the Voigt notations of the Green-Lagrange strain tensor and the second Piola-Kirchhoff stress tensor, respectively, and W, H, and L are the width, height, and length of the beam, respectively. The evaluation of the determinant $J_0 = \det\left(\mathbf{J}_0\right) = \det\left(\partial\mathbf{X}/\partial\mathbf{x}\right)$ is required in the case of initially curved reference configuration,

$\mathbf{X} = \mathbf{S}\mathbf{e}_0$ is the vector of the parameters in the stress-free reference configuration, and $\mathbf{x}$ is the vector of the element coordinates in the straight configuration. The constitutive relations can be written in terms of the elastic coefficient matrix $\mathbf{D}$ as $\boldsymbol{\sigma}_{P2} = \mathbf{D}\boldsymbol{\varepsilon}$, where $\mathbf{D}$ is given in the Appendix in the case of the general continuum mechanics approach. The generalized elastic forces can be obtained by differentiating the strain energy with respect to the nodal coordinates. The strain energy in the case of the enhanced continuum mechanics approach can be written as

$$U_E = \frac{1}{2}\int_{-W/2}^{W/2}\int_{-H/2}^{H/2}\int_{0}^{L}\boldsymbol{\varepsilon}^T\mathbf{D}^0\boldsymbol{\varepsilon}J_0 dxdydz + \frac{1}{2}HW\int_{0}^{L}\boldsymbol{\varepsilon}^T\mathbf{D}^v\boldsymbol{\varepsilon}J_0 dx \tag{26}$$

The elasticity matrices $\mathbf{D}^0$ and $\mathbf{D}^v$ are provided in the Appendix. Both, the general continuum mechanics and enhanced continuum mechanics approaches are used in this investigation to evaluate the elastic forces of the proposed elements.

The kinematics of the elements developed in this paper significantly influence the element performance. The low order element in particular cannot assume complex shapes and it is necessary in some application to use a large number of elements. Because the curvature inside this element is identically zero, classical beam theories that require the use of the differential geometry curvature definitions cannot be used with this low order element (Zheng et al., 2018). Figure 2 shows the three different elements developed in this investigation and their nodal coordinates. Table 1 shows a comparison between all the elements considered in this study.

7. NUMERICAL RESULTS AND DISCUSSION

The higher order ANCF/CRBF elements, *ANCF/CRBF18* and *ANCF/CRBF14*, ensure continuity of the rotation and stress fields at the nodal points, while the lower order elements, *LINBEAM18* and *CRBF12*, do not ensure continuity of $\mathbf{r}_x$ and hence only position and rotation field continuity

is ensured at the nodes. The numerical results obtained from all the proposed elements are validated against the results obtained using the fully parameterized ANCF beam element (*ANCF24*) and a beam element implemented in the commercial FE software ANSYS. Both static and dynamic examples are considered in this study for validation of the numerical results. The static analysis include validation for a small deformation and a large deformation cantilever beam problem. Simulation of a beam pendulum falling under the effect of gravity is performed in order to evaluate the dynamic performance of the element. A detailed convergence analysis of the displacement and strain variables is performed. A simulation time study is presented at the end of the section to analyze element efficiency using different geometric and material properties.

7.1 Static Analysis

A cantilever beam problem is considered in this section in which one end of the beam is fixed and a vertical tip load is applied at the free end as shown in Fig. 3. Two cases are considered, a small deformation problem and a large deformation problem, both of which are considered in the literature (Nachbagauer et al., 2013). The beams analyzed in this problem have Young's modulus $E = 2.07\times10^{11}$ Pa, Poisson ratio $\nu = 0.3$, length $L = 2$ m, width $W = 0.5$ m, and height $H = 0.1$ m. For the small deformation problem, the analytical solution for the vertical displacement of the tip u_y is given in Timoshenko and Goodier (1970) as

$$u_y = -\frac{P}{6EI}\left[(4+5\nu)\frac{W^2L}{4} + 2L^3\right] \tag{27}$$

where I is the second moment of area of the cross-section, and P is the vertical applied tip load. Considering the above-mentioned parameters and a tip load $P = 6.25\times10^4$ N, the vertical tip displacement value is $u_y = -8.06159\times10^{-4}$ m. The commercial FE software ANSYS yields vertical tip displacement equal to -8.1024×10^{-4} m. Table 2 shows the results obtained for this

problem using the higher order elements *ANCF24*, *ANCF/CRBF18*, and *ANCF/CRBF14*, while Table 3 shows the numerical results obtained for the linear elements, *LINBEAM18* and *CRBF12*. As can be observed from these numerical results, with the general continuum mechanics approach an under-predicted solution is obtained due to the locking effect. However, with the enhanced continuum mechanics, the solutions obtained by all elements match the analytical value as well as the solution given by the commercial FE software. It can be observed that the convergence rate for the *ANCF24* and both *ANCF/CRBF* elements is comparable and these elements require around fifteen elements to achieve convergence. In case of the linear elements, the convergence properties of the *LINBEAM18* and *CRBF12* are very similar.

In the large-deformation cantilever beam problem, the tip load value is increased to $P = 6.25 \times 10^7 \,\mathrm{N}$ and the remaining beam properties are kept the same. The beam element BEAM188 implemented in the commercial software ANSYS gives a vertical tip displacement solution of $-0.71131 \,\mathrm{m}$. Tables 4 and 5 show the results obtained for the large deformation problem using the higher order and linear elements, respectively. As can be observed, when the general continuum mechanics approach is used, the locking effect has an impact on the solution of the ANCF/CRBF and the CRBF elements. When the locking effect is alleviated using the enhanced continuum mechanics approach, the solutions obtained using all the presented elements become close to the solution predicted using the commercial FE software. The *ANCF/CRBF14* element under-predicts the solution by a small amount as compared to the other elements due to elimination of deformation modes resulting from the orthogonality condition imposed on the nodal position vector gradients. The shear effect at nodes cannot be captured with this element as previously mentioned. With regard to the linear elements, the tip vertical displacement obtained from *LINBEAM18* element compares well with the solution of the *ANCF24* element, whereas the small

difference between the solutions of the *LINBEAM18* and *CRBF12* elements can be justified because of the rigidity of the cross-section of the *CRBF12* element. As expected in case of a large deformation nonlinear problem, all elements exhibit different convergence rates.

7.2 Dynamic Analysis

A beam pendulum problem is considered in order to demonstrate the ability of the proposed elements to handle large-rotation and large-deformation MBS applications. The beam pendulum, shown in Fig. 3, which has one end attached to a support using a spherical joint, is allowed to fall under the effect of gravity. The beam considered in this problem has Young's modulus $E = 2\times10^7$ Pa, Poisson ratio $\nu = 0.3$, density $\rho = 7200$ kg/m^3, length $L = 1$ m, and width and height $W = H = 0.02$ m. The general continuum mechanics approach is used in this case to evaluate the element elastic forces. The time span considered for the numerical simulations is 2 seconds and a variable-step, variable-order Adams-Bashforth-Moulton PECE integrator is used to solve the equations of motion (Shampine and Gordon, 1975).

The results of the higher order ANCF/CRBF elements are analyzed first. Figure 4 shows the comparison of converged results for the x displacements of the tip of the pendulum for the *ANCF24* beam, the higher order ANCF/CRBF elements, and the element implemented in the commercial FE software. As can be seen, the solutions obtained from the proposed elements agree well with the solutions obtained from the *ANCF24* element and the commercial FE software. As shown in Fig. 5, the displacement convergence rate for the *ANCF/CRBF18* and *ANCF/CRBF14* elements is comparable. Normalized RMS error against number of elements employed in the solution is used as a convergence rate measure. The converged *ANCF24* solution is used as the reference solution while computing the normalized RMS error. As observed, the displacement convergence rate for both the higher order ANCF/CRBF elements is very similar. The convergence

of the longitudinal strain at the center of the *ANCF24* beam pendulum is presented in Fig. 6 to establish a reference for assessing the longitudinal strain convergence of the proposed elements. Converged longitudinal strain results are compared for both the ANCF/CRBF elements in Fig. 7, and as can be observed there is a close match between the two. Figure 8 shows the longitudinal strain normalized RMS error for the ANCF/CRBF higher order elements. It is clear that both the elements have similar longitudinal strain convergence rate. However, the normalized longitudinal strain RMS error value is slightly higher, which can be attributed to the fact that the cross-section of the ANCF/CRBF elements is rigid at the nodes and Poisson coupling affects strain values. This error significantly decreases if zero Poisson ratio is considered. Shear strain convergence is shown in Fig. 9 for the *ANCF24* element to establish base for convergence analysis of the shear-deformable *ANCF/CRBF18* element. As can be seen in Fig. 10, the converged shear strain results for the *ANCF24* and *ANCF/CRBF18* elements show a good agreement. In Fig. 11, the *ANCF/CRBF18* element shear strain convergence rate is presented where the normalized RMS error stabilizes to a small value as the number of elements increases. As expected, more *ANCF/CRBF18* elements are required compared to the more general *ANCF24* element to achieve converged shear strain results.

Figure 12 compares the time histories of the pendulum tip displacement predicted using the linear beam elements, *LINBEAM18* and *CRBF12*, and the *ANCF24* element. There is a good agreement between the converged displacements of the linear elements and the *ANCF24* element. As shown in Fig. 13, the *LINBEAM18* beam has a similar displacement convergence rate as the *CRBF12* element. Since there is no constraint on the transverse position vector gradients in case of the *LINBEAM18*, the longitudinal strain obtained for this element shows a reasonable agreement with the results of the *ANCF24* element as demonstrated in Fig. 14. The decreasing normalized

RMS error for the longitudinal strain of the *LINBEAM18* element demonstrates a good convergence rate as observed from the results of Fig. 15. The *LINBEAM18* element requires a much finer mesh to produce converged results as compared to the higher order elements due to the linear interpolation field. Figure 16 shows the longitudinal strain time histories predicted using the *CRBF12* and the *ANCF/CRBF18* elements. It is observed that the *CRBF12* strain follows the same trend as the *ANCF/CRBF18* strain but tends to deviate slightly towards the end of the simulation. This can be justified because of the significant difference between the kinematic descriptions of these elements and the order of the polynomial interpolation, as well as the lack of longitudinal position vector gradient continuity in the case of the *CRBF12* element. The *CRBF12* element longitudinal strain RMS error is shown in Fig. 17.

7.3 Simulation Time Study

In order to compare simulation times for different beam geometries and material properties, two sets of simulations for the pendulum problem are performed. In the first set, which has a beam with a thicker cross section, the following properties are used: Young's modulus $E = 2\times10^6$ Pa, Poisson ratio $\nu = 0$, density $\rho = 5400$ kg/m^3, length $L = 2$ m, and width and height $W = H = 0.1$ m. The second simulation set has a beam Young's modulus $E = 2\times10^7$ Pa, Poisson ratio $\nu = 0.3$, length $L = 1$ m, and a relatively thinner cross-section 0.02×0.02 m^2. Tables 6 and 7 show the CPU times for the two simulation sets. It is observed that for the beam set having a thick cross-section of 0.1×0.1 m^2, the *ANCF24* element model is always more efficient than the higher order *ANCF/CRBF* elements, and similarly the *LINBEAM18* element is always more efficient than the *CRBF12* element. However, in the case of a slender beam (the second set), for a smaller number of elements, the *ANCF/CRBF* elements tend to be more efficient than the *ANCF24* element, and similarly the *CRBF12* is more efficient than the *LINBEAM18* beam. As the mesh is

refined, the gradient-based elements, *ANCF24* and *LINBEAM18*, become more efficient as the mass matrix nonlinearity impacts the simulation speed of the rotation-based elements.

8. SUMMARY AND CONCLUSIONS

Starting with the kinematic description of the ANCF elements, several new CRBF beam elements were developed in this investigation. These elements employ rotation parameters as nodal coordinates without the need for the use of independent interpolation of the rotation field. Only one interpolation position field is used in order to ensure consistency with the principles of continuum mechanics and avoid the redundancy problems associated with other finite rotation-based formulations. Furthermore, the kinematic description used for the new elements allows for describing arbitrarily large displacements, and therefore, the resulting equations can be solved non-incrementally, eliminating the need for using the co-rotational procedures. The transverse position vector gradients are expressed as orthogonal unit vectors in terms of finite rotation parameters at nodal points, thereby eliminating high frequency modes associated with the cross-section deformation. The time derivatives of the position vector gradients were expressed in terms of the time derivatives of the orientation parameters using a velocity transformation matrix. Acceleration-level equations were obtained for all the proposed elements. As demonstrated by the static and dynamic simulations performed in this investigation, the proposed CRBF elements yield results which agree well with the original ANCF elements and with a beam element implemented in a commercial FE software. Displacement and longitudinal strain comparisons were made for all the proposed elements, and the comparative study showed a good agreement for the displacements obtained. There is a slight discrepancy observed in the case of longitudinal strains which can be attributed to the Poisson effect and the assumption of the rigidity of the cross-section. The shear

strain results obtained using the higher order shear-deformable ANCF/CRBF element were found to be in a good agreement with the results of the ANCF beam element. The linear CRBF element requires higher number of elements to achieve converged displacement and strain results. The gradient continuity along the longitudinal direction is not ensured in the case of the linear elements, and because these elements employ linear polynomial interpolations, a high number of elements may be required to achieve good results for complex nonlinear geometries. Nonetheless, these elements are efficient and can yield acceptable displacement results, while strain results may not be accurate. A simulation time comparison was performed to shed light on the computational efficiency of the proposed elements with beams having different geometries and material properties. It was found that for thick beams, the gradient-based elements are always more efficient than the proposed consistent rotation-based elements. However, for slender beams and smaller mesh sizes, the proposed rotation-based elements tend to be more efficient up to the point at which the nonlinearity of the mass matrix starts to negatively impact the simulation efficiency when finer mesh sizes are used.

APPENDIX

Elasticity Matrices- General and Enhanced Continuum Mechanics Approaches

The elasticity matrix used in the linear elastic constitutive material model is given by

$$\mathbf{D}=\frac{E\nu}{(1+\nu)(1-2\nu)}\begin{bmatrix} \frac{1-\nu}{\nu} & 1 & 1 & 0 & 0 & 0 \\ 1 & \frac{1-\nu}{\nu} & 1 & 0 & 0 & 0 \\ 1 & 1 & \frac{1-\nu}{\nu} & 0 & 0 & 0 \\ 0 & 0 & 0 & \frac{1-2\nu}{2\nu} & 0 & 0 \\ 0 & 0 & 0 & 0 & \frac{1-2\nu}{2\nu} & 0 \\ 0 & 0 & 0 & 0 & 0 & \frac{1-2\nu}{2\nu} \end{bmatrix} \tag{A.1}$$

where ν is the Poisson ratio. In the general continuum mechanics approach, the axial and the transverse normal strains are coupled using the Poisson ratio. This effect causes Poisson locking and as recommended in the literature (Nachbagauer et al., 2013) the elasticity matrix is split into two parts as $\mathbf{D}=\mathbf{D}^0+\mathbf{D}^\nu$, where $\mathbf{D}^0$ does not include the Poisson ratio and can be written as $\mathbf{D}^0=diag(E,E,E,Gk_2,Gk_3,G)$, where G is the shear modulus and k_2 and k_3 are the shear correction factors. The matrix $\mathbf{D}^\nu$ includes the Poisson terms and is given by,

$$\mathbf{D}^\nu=\frac{E\nu}{(1+\nu)(1-2\nu)}\begin{bmatrix} 2\nu & 1 & 1 & 0 & 0 & 0 \\ 1 & 2\nu & 1 & 0 & 0 & 0 \\ 1 & 1 & 2\nu & 0 & 0 & 0 \\ 0 & 0 & 0 & 0 & 0 & 0 \\ 0 & 0 & 0 & 0 & 0 & 0 \\ 0 & 0 & 0 & 0 & 0 & 0 \end{bmatrix} \tag{A.2}$$

REFERENCES

1. Bathe, K.J., 1996, *Finite Element Procedures*, Prentice Hall, Inc., Englewood Cliffs, New Jersey.
2. Belytschko, T. and Hsieh, B.J., 1973, "Non-linear transient finite element analysis with convected co-ordinates", *International Journal for Numerical Methods in Engineering*, *7*(3), pp.255-271.
3. Belytschko, T., Liu, W.K., and Moran, B., 2000, *Nonlinear Finite Elements for Continua and Structures*, John Wiley & Sons, New York.
4. Bonet, J., and Wood, R.D., 1997, *Nonlinear Continuum Mechanics for Finite Element Analysis*, Cambridge University Press.
5. Campanelli, M., Berzeri, M., and Shabana, A.A., 2000, "Performance of the incremental and non-incremental finite element formulations in flexible multibody problems", *Transactions-American Society of Mechanical Engineers Journal of Mechanical Design*, 122(4), pp.498-507.
6. Cook, R.D., Malkus, D.S., and Plesha, M.E., 1989, *Concepts and Applications of Finite Element Analysis*, Third Edition, John Wiley & Sons.
7. Crisfield, M.A., 1991, *Nonlinear Finite Element Analysis of Solids and Structures, Vol. 1: Essentials*, John Wiley & Sons.
8. Ding, J., Wallin, M., Wei, C., Recuero, A. M., and Shabana, A. A., 2014, "Use of Independent Rotation Field in the Large Displacement Analysis of Beams", *Nonlinear Dynamics*, 76, pp. 1829-1843.

9. Dmitrochenko, O., and Mikkola, A., 2011, "Digital Nomenclature Code for Topology and Kinematics of Finite Elements Based on the Absolute Nodal Co-Ordinate Formulation", *IMechE Journal of Multibody Dynamics*, Vol. 225, pp. 34-51.
10. Gerstmayr, J., Gruber, P. and Humer, A., 2017, "Comparison of Fully Parameterized and Gradient Deficient Elements in the Absolute Nodal Coordinate Formulation", *ASME 2017 International Design Engineering Technical Conferences and Computers and Information in Engineering Conference*, pp. V006T10A025-V006T10A025.
11. Gerstmayr, J., and Irschik, H., 2008, "On the Correct Representation of Bending and Axial Deformation in the Absolute Nodal Coordinate Formulation with an Elastic Line Approach," *Journal of Sound & Vibration*, 318(3), pp. 461-487.
12. Gerstmayr, J., Matikainen, M.K., and Mikkola, A.M., 2008, "A geometrically exact beam element based on the absolute nodal coordinate formulation", *Multibody System Dynamics*, 20(4), pp.359-384.
13. Greenberg, M. D., 1998, *Advanced Engineering Mathematics*, *Second Edition*, Prentice-Hall, Englewood Cliffs, NJ.
14. Gruber, P.G., Nachbagauer, K., Vetyukov, Y. and Gerstmayr, J., 2013, "A novel director-based Bernoulli–Euler beam finite element in absolute nodal coordinate formulation free of geometric singularities", *Mechanical Sciences*, *4*(2), pp.279-289.
15. Hu, W., Tian, Q., and Hu, H. Y., 2014, "Dynamics Simulation of the Liquid-Filled Flexible Multibody System via the Absolute Nodal Coordinate Formulation and SPH Method", *Nonlinear Dynamics*, Vol. 75, pp. 653-671.
16. Kreyszig, E., 1991, *Differential Geometry*, Dover Publications.

17. Kulkarni, S., Pappalardo, C. M., and Shabana, A. A., 2017, "Pantograph/Catenary Contact Formulations", *ASME Journal of Vibrations and Acoustics*, 139(1), pp. 1-12.

18. Liu, C., Tian, Q., and Hu, H. Y., 2011, "Dynamics of Large Scale Rigid-Flexible Multibody System Composed of Composite Laminated Plates", *Multibody System Dynamics*, Vol. 26, pp. 283-305.

19. Matikainen, M.K., von Hertzen, R., Mikkola, A. and Gerstmayr, J., 2010, "Elimination of high frequencies in the absolute nodal coordinate formulation", *Proceedings of the Institution of Mechanical Engineers, Part K: Journal of Multi-body Dynamics*, 224(1), pp.103-116.

20. Nachbagauer, K., 2013, "Development of Shear and Cross-Section Deformable Beam Finite Elements Applied to Large Deformation and Dynamics Problems", Ph.D. dissertation, Johannes Kepler University, Linz, Austria.

21. Nachbagauer, K., Pechstein, A.S., Irschik, H., and Gerstmayr, J., 2011, "A new locking-free formulation for planar, shear deformable, linear and quadratic beam finite elements based on the absolute nodal coordinate formulation", *Multibody System Dynamics*, 26(3), pp.245-263.

22. Nachbagauer, K., Gruber, P., and Gerstmayr, J., 2013, "Structural and continuum mechanics approaches for a 3D shear deformable ANCF beam finite element: application to static and linearized dynamic examples", *Journal of Computational and Nonlinear Dynamics*, 8(2), pp. 021004-1 - 021004-7.

23. Nachbagauer, K., 2014, "State of the art of ANCF elements regarding geometric description, interpolation strategies, definition of elastic forces, validation and the locking phenomenon in comparison with proposed beam finite elements", *Archives of Computational Methods in Engineering*, 21(3), pp.293-319.

24. Nicolsen, B., Wang L., and Shabana, A. A., 2017, "Nonlinear Finite Element Analysis of Liquid Sloshing in Complex Vehicle Motion Scenarios", *Journal of Sound and Vibration*, 405, pp. 208-233.
25. Orzechowski G., 2012, "Analysis of Beam Elements of Circular Cross-Section Using The Absolute Nodal Coordinate Formulation", *Archive of Mechanical Engineering*, Vol. 59, pp. 283-296.
26. Orzechowski G., Frączek J., 2012, "Integration of The Equations of Motion of Multibody Systems Using Absolute Nodal Coordinate Formulation", *Acta Mechanica et Automatica*, Vol. 6, pp. 75-83.
27. Orzechowski G., Frączek J., 2015, "Nearly Incompressible Nonlinear Material Models in The Large Deformation Analysis of Beams Using ANCF", *Nonlinear Dynamics*, pp. 1-14.
28. Pappalardo, C. M., 2015, "A Natural Absolute Coordinate Formulation for the Kinematic and Dynamic Analysis of Rigid Multibody Systems", *Journal of Nonlinear Dynamics*, 81, pp. 1841-1869.
29. Pappalardo, C. M., Wallin, M., and Shabana, A. A., 2017, "A New ANCF/CRBF Fully Parametrized Plate Finite Element", *ASME Journal of Computational and Nonlinear Dynamics*, 12(3), pp. 1-13.
30. Patel, M. D., Orzechowski, G., Tian, Q., and Shabana, A. A., 2015, "A New Multibody System Approach for Tire Modeling using ANCF Finite Elements", *Proceedings of the Institution of Mechanical Engineers, Part K: Journal of Multi-body Dynamics*, 0(0), 1-16.
31. Patel, M. and Shabana, A.A., 2018, "Locking alleviation in the large displacement analysis of beam elements: the strain split method", *Acta Mechanica*, accepted for publication.

32. Rankin, C. C., and Brogan, F. A., 1986, "An Element Independent Corotational Procedure for the Treatment of Large Rotations'', *ASME J. Pressure Vessel Technol*., 108, pp. 165–174.
33. Roberson, R. E., and Schwertassek, R., 1988, *Dynamics of Multibody Systems*, Springer, Berlin, Germany.
34. Shabana, A. A., 2010, "Uniqueness of the geometric representation in large rotation finite element formulations", *Journal of Computational and Nonlinear Dynamics*, *5*(4), pp. 044501-1 – 44501-5.
35. Shabana, A. A., 2013, *Dynamics of Multibody Systems*, *Fourth Edition*, Cambridge University Press, Cambridge, United Kingdom.
36. Shabana, A. A., 2016, "ANCF Consistent Rotation-Based Finite Element Formulation", *ASME Journal of Computational and Nonlinear Dynamics*, 11(1), pp. 014502-1 - 014502-4.
37. Shabana, A.A. and Patel, M., 2018, "Coupling between shear and bending in the analysis of beam problems: Planar case", *Journal of Sound and Vibration*, *419*, pp.510-525.
38. Shabana, A.A., and Yakoub, R.Y., 2001, "Three-dimensional absolute nodal coordinate formulation for beam elements: Theory", *Transactions-American Society of Mechanical Engineers Journal of Mechanical Design*, 123(4), pp.606-613.
39. Shampine, L., and Gordon, M., 1975, *Computer Solution of ODE: The Initial Value Problem*, Freeman, San Francisco.
40. Simo, J. C., and Vu-Quoc, L., 1986, "On the Dynamics of Flexible Beams under Large Overall Motions - The Plane Case, Part I", *Journal of Applied Mechanics*, 53, pp. 849-863.
41. Takahashi, Y. and Shimizu, N., 1999, Study on Elastic Forces of the Absolute Nodal Coordinate Formulation for Deformable Beams, *Proc. ASME International Design*

Engineering Technical Conferences and Computer and Information in Engineering Conference, Las Vegas, NV.

42. Tian, Q., Chen, L. P., Zhang, Y. Q., and Yang, J. Z., 2009, "An Efficient Hybrid Method for Multibody Dynamics Simulation Based on Absolute Nodal Coordinate Formulation", *ASME Journal of Computational and Nonlinear Dynamics*, Vol. 4, pp. 021009-1 - 021009-14.
43. Tian, Q., Sun, Y. L., Liu, C., Hu, H. Y., and Paulo, F., 2013, "Elasto-Hydro-Dynamic Lubricated Cylindrical Joints for Rigid-Flexible Multibody Dynamics", *Computers & Structures*, Vol. 114-115, pp. 106-120.
44. Timoshenko, S.P., and Goodier, J.N., 1970, "Theory of elasticity", McGraw-Hill Book Co., Inc., New York.
45. Wittenburg, J., 2007, *Dynamics of Multibody Systems*, *Second Edition*, Springer, Berlin, Germany.
46. Yakoub, R.Y., and Shabana, A.A., 2001, "Three dimensional absolute nodal coordinate formulation for beam elements: implementation and applications", *Transactions-American Society of Mechanical Engineers Journal of Mechanical Design*, 123(4), pp.614-621.
47. Zheng, Y., and Shabana, A.A., 2017, "A two-dimensional shear deformable ANCF consistent rotation-based formulation beam element", *Nonlinear Dynamics*, 87(2), pp.1031-1043.
48. Zheng, Y., Shabana, A.A., and Zhang, D., 2018, "Curvature Expressions for the Large Displacement Analysis of Planar Beam Motions", *ASME Journal of Computational and Nonlinear Dynamics*, Vol. 13, pp. 011013-1 – 011013-12.
49. Zienkiewicz, O.C., 1977, *The Finite Element Method*, Third Edition, McGraw Hill, New York.
50. Zienkiewicz, O.C., and Taylor, R.L., 2000, *The Finite Element Method, Vol. 2: Solid Mechanics*, Fifth Edition, Butterworth Heinemann.

List of Figures

Figure 17. Longitudinal strain normalized RMS error for CRBF12 element

Table 1. ANCF and ANCF/CRBF element comparison

Element Property	**ANCF24**	**ANCF/CRBF18**	**ANCF/CRBF14**	**LINBEAM18**	**CRBF12**
Nodal coordinates	Positions and gradient vectors in all three directions	Positions, longitudinal gradient vector, and angles	Positions, angles, and extensibility parameter along longitudinal axis	Positions and transverse gradient vectors	Positions and angles
Number of element coordinates	24	18	14	18	12
Order of interpolation along longitudinal axis	Cubic	Cubic	Cubic	Linear	Linear
Order of interpolation along transverse axes	Linear	Linear	Linear	Linear	Linear
Shear deformation	Yes	Yes	No	Yes	Yes
Bending deformation	Yes	Yes	Yes	No	No
Stretch deformation	Yes	Yes	Yes	Yes	Yes
Torsional deformation	Yes	Yes	Yes	Yes	Yes
Cross-section deformation	Yes	No	No	Yes	No
Strain continuity	Yes	Yes	Yes	No	No

Table 2. Small deformation cantilever beam problem tip vertical displacements in meters-

Elements	ANCF24		ANCF/CRBF18		ANCF/CRBF14	
	General Continuum	Enhanced Continuum	General Continuum	Enhanced Continuum	General Continuum	Enhanced Continuum
5	-5.9911E-04	-8.0201E-04	-5.9911E-04	-8.0201E-04	-5.9461E-04	-7.9662E-04
10	-6.0378E-04	-8.0825E-04	-6.0378E-04	-8.0825E-04	-5.9892E-04	-8.0242E-04
15	-6.0471E-04	-8.0947E-04	-6.0471E-04	-8.0947E-04	5.9972E-04	-8.0349E-04
20	-6.0505E-04	-8.0992E-04	-6.0505E-04	-8.0992E-04	-6.0000E-04	-8.0386E-04
25	-6.0521E-04	-8.1014E-04	-6.0521E-04	-8.1014E-04	-6.0013E-04	-8.0404E-04
30	-6.0531E-04	-8.1027E-04	-6.0531E-04	-8.1027E-04	-6.0020E-04	-8.0413E-04
35	-6.0537E-04	-8.1034E-04	-6.0537E-04	-8.1034E-04	-6.0024E-04	-8.0419E-04
40	-6.0541E-04	-8.1040E-04	-6.0541E-04	-8.1040E-04	-6.0027E-04	-8.0423E-04

Table 3. Small deformation cantilever beam problem tip vertical displacements in meters-

Elements	LINBEAM18		CRBF12	
	General Continuum	Enhanced Continuum	General Continuum	Enhanced Continuum
10	-5.7912E-04	-7.7109E-04	-5.7912E-04	-7.7109E-04
20	-5.9875E-04	-8.0037E-04	-5.9875E-04	-8.0037E-04
40	-6.0386E-04	-8.0804E-04	-6.0386E-04	-8.0804E-04
60	-6.0482E-04	-8.0947E-04	-6.0482E-04	-8.0947E-04
80	-6.0516E-04	-8.0998E-04	-6.0516E-04	-8.0998E-04
100	-6.0531E-04	-8.1021E-04	-6.0531E-04	-8.1021E-04
120	-6.0540E-04	-8.1034E-04	-6.0540E-04	-8.1034E-04
140	-6.0545E-04	-8.1042E-04	-6.0545E-04	-8.1042E-04

Table 4. Large deformation cantilever beam problem tip vertical displacements in meters-

Elements	ANCF24		ANCF/CRBF18		ANCF/CRBF14	
	General Continuum	Enhanced Continuum	General Continuum	Enhanced Continuum	General Continuum	Enhanced Continuum
10	-0.561554634	-0.712463018	-0.55630973	-0.705176357	-0.552383366	-0.70109317
20	-0.562793972	-0.714094246	-0.558952941	-0.708529064	-0.554745158	-0.704029801
30	-0.563070396	-0.714463954	-0.5598123	-0.709741826	-0.555528786	-0.705140965
40	-0.563182513	-0.714615838	-0.560230427	-0.710347297	-0.555911812	-0.705701245
60	-0.563276796	-0.714744706	-0.560638531	-0.710946329	-0.556286462	-0.706258417
80	-0.56331709	-0.714800073	-0.560838268	-0.711242035	-0.556470044	-0.706534344
100	-0.563339031	-0.714830262	-0.560956601	-0.711417914	-0.556578855	-0.7066987
120	-0.563352715	-0.714849094	-0.561034831	-0.711534447	-0.556650806	-0.70680769

Table 5. Large deformation cantilever beam problem tip vertical displacements in meters-

Elements	LINBEAM18		CRBF12	
	General Continuum	Enhanced Continuum	General Continuum	Enhanced Continuum
20	-0.557828944	-0.707665414	-0.554101713	-0.702249911
40	-0.562003027	-0.713092558	-0.559083546	-0.708866867
60	-0.562783387	-0.714109553	-0.560163466	-0.710334906
80	-0.563057139	-0.714466747	-0.560591127	-0.71092506
100	-0.563183965	-0.714632336	-0.560811415	-0.711232472
120	-0.563252891	-0.71472236	-0.560943066	-0.711417822
140	-0.563294462	-0.714776669	-0.56102963	-0.711540577
160	-0.563321448	-0.714811928	-0.561090457	-0.711627355

Table 6. CPU time (s) comparison for thick beam geometry

Elements	ANCF24	ANCF/CRBF18	ANCF/CRBF14	LINBEAM18	CRBF12
1	11.623	11.596	7.012	7.410	7.247
5	55.357	59.604	48.613	34.082	39.068
15	378.821	420.711	381.033	120.938	132.092
25	1003.928	1206.375	1079.887	268.585	292.275
35	2056.425	2764.407	2510.736	488.024	566.244
45	3489.381	5061.560	4506.753	759.079	953.694
55	5471.129	8524.073	7254.975	1197.076	1672.551

Table 7. CPU time (s) comparison for thin beam geometry

Elements	ANCF24	ANCF/CRBF18	ANCF/CRBF14	LINBEAM18	CRBF12
1	224.146	114.151	18.809	165.359	81.404
5	629.860	389.228	171.531	396.917	207.660
15	1875.058	1631.783	1207.202	951.967	679.977
25	3492.149	3933.574	3759.607	1593.738	1312.408
35	7341.493	9709.677	8656.744	2332.738	2374.667
45	12461.359	16931.749	14191.537	3230.719	3668.342
55	18738.160	28308.096	23652.541	4876.967	5846.339

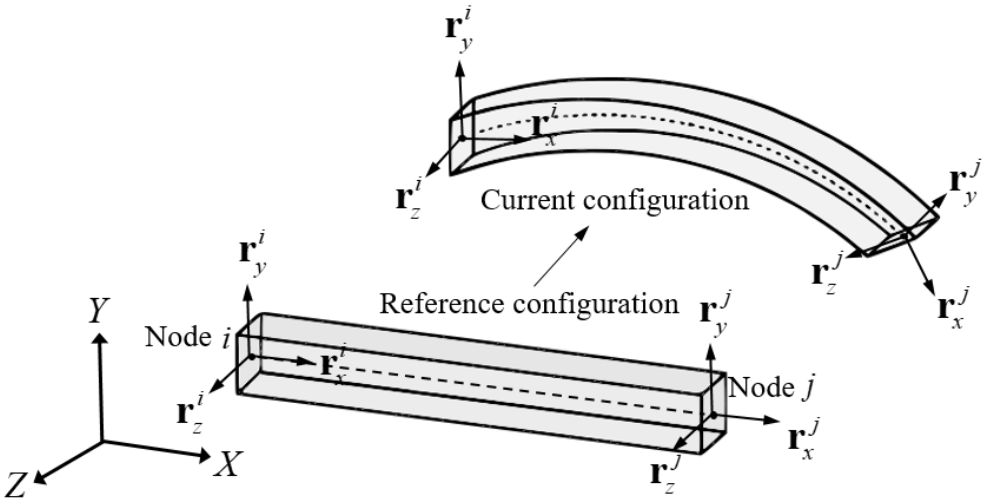

Figure 1. Three-dimensional ANCF fully parameterized beam element

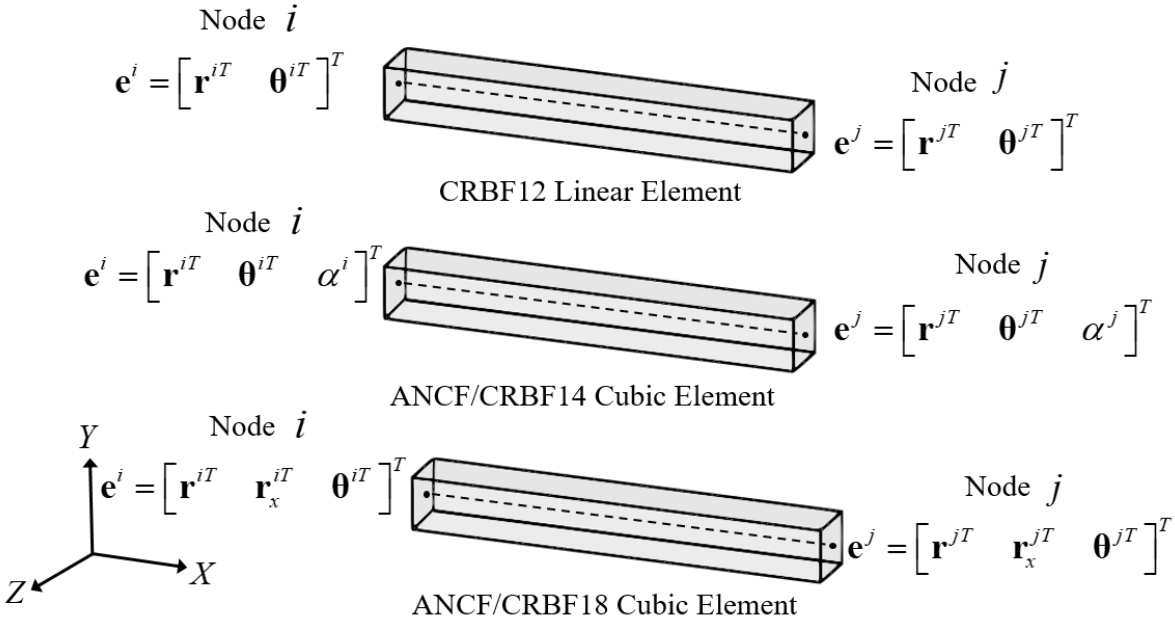

Figure 2. Element coordinates

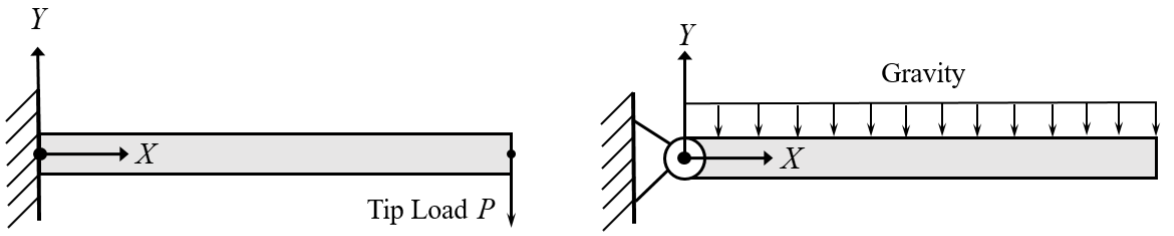

(a) Static problem- cantilever beam (b) Dynamic problem- pendulum under gravity

Figure 3. Numerical tests on proposed elements

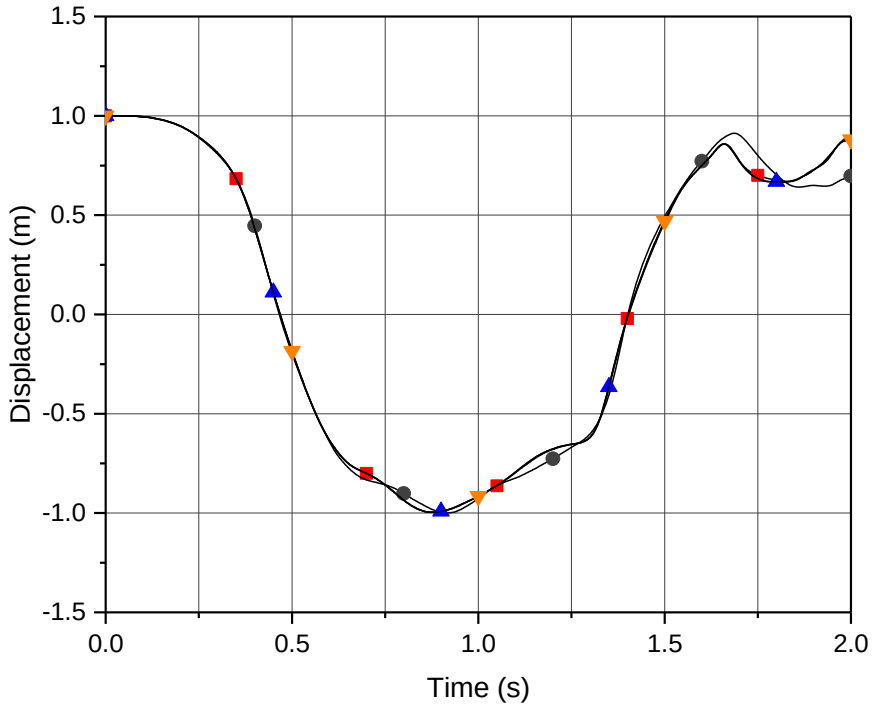

Figure 4. Pendulum tip X -displacement comparison (25 ANCF24 elements, 25 ANCF/CRBF18 elements, 25 ANCF/CRBF14 elements, 25 Commercial FE code beam elements)

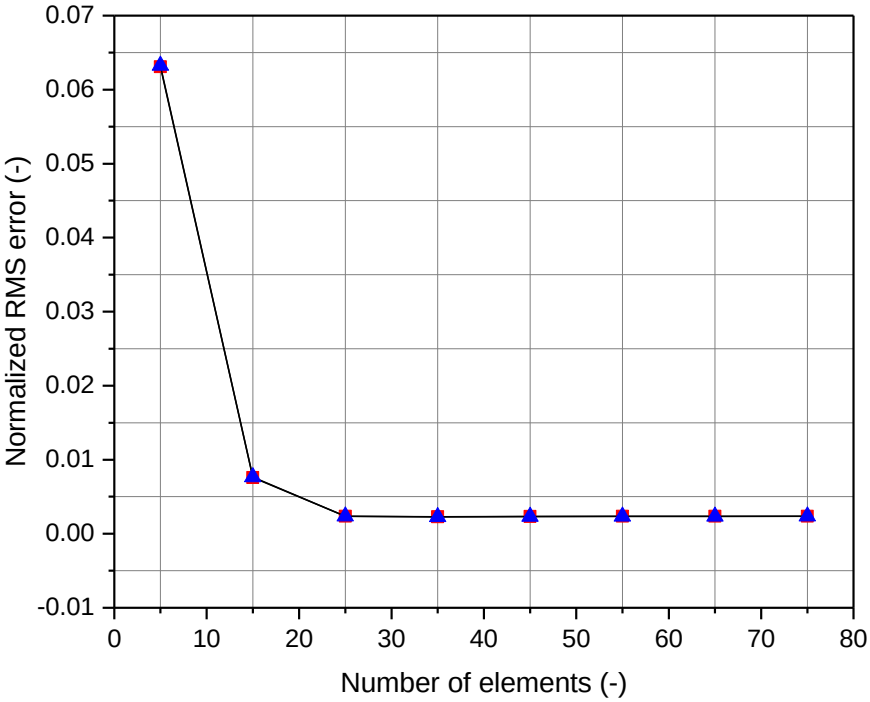

Figure 5. Tip X -displacement normalized RMS error for higher order ANCF/CRBF elements

(ANCF/CRBF18 element, ANCF/CRBF14 element)

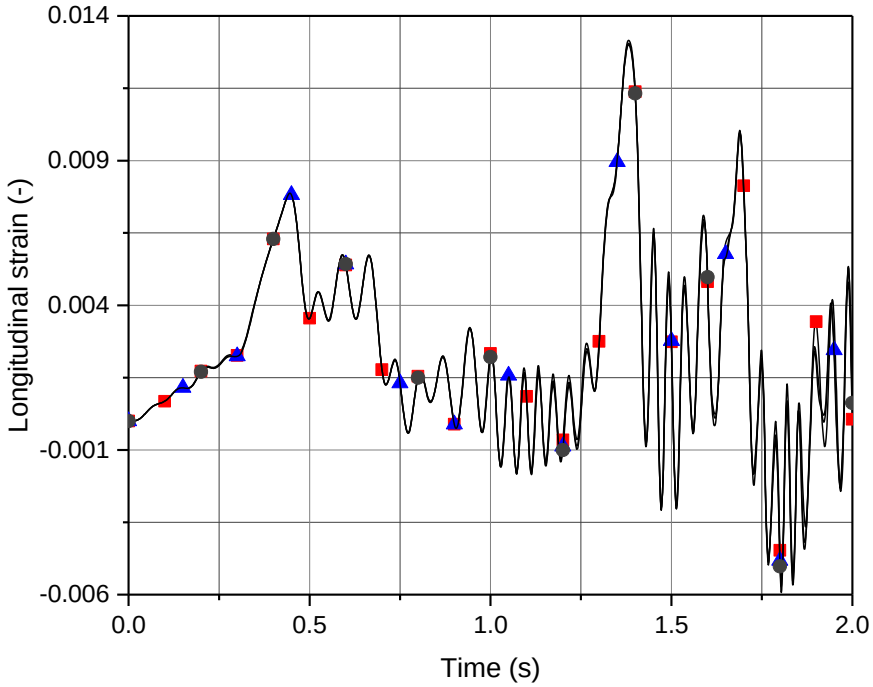

Figure 6. Longitudinal strain convergence for ANCF24 element (25 elements, 35 elements, 45 elements)

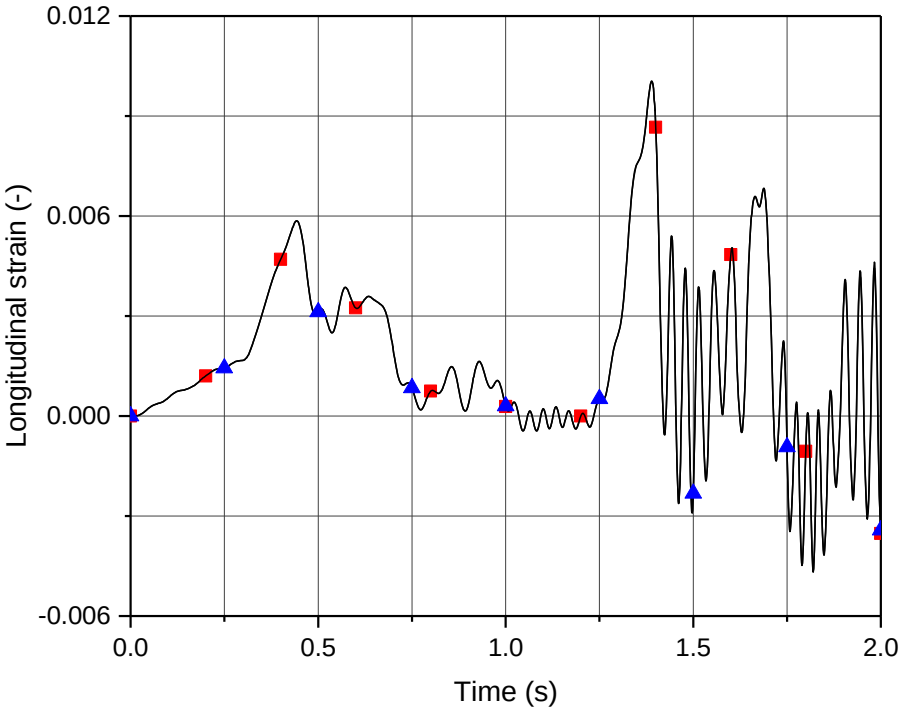

Figure 7. Longitudinal strain comparison between higher order ANCF/CRBF elements
(—■— 55 ANCF/CRBF18 elements, —▲— 55 ANCF/CRBF14 elements)

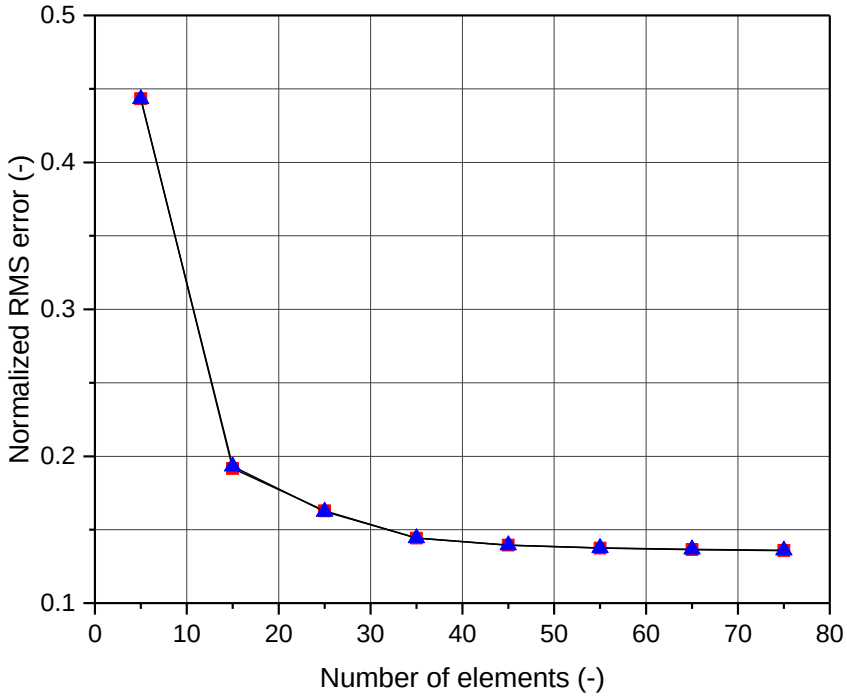

Figure 8. Longitudinal strain normalized RMS error for higher order ANCF/CRBF elements
(—■— ANCF/CRBF18 element, —▲— ANCF/CRBF14 element)

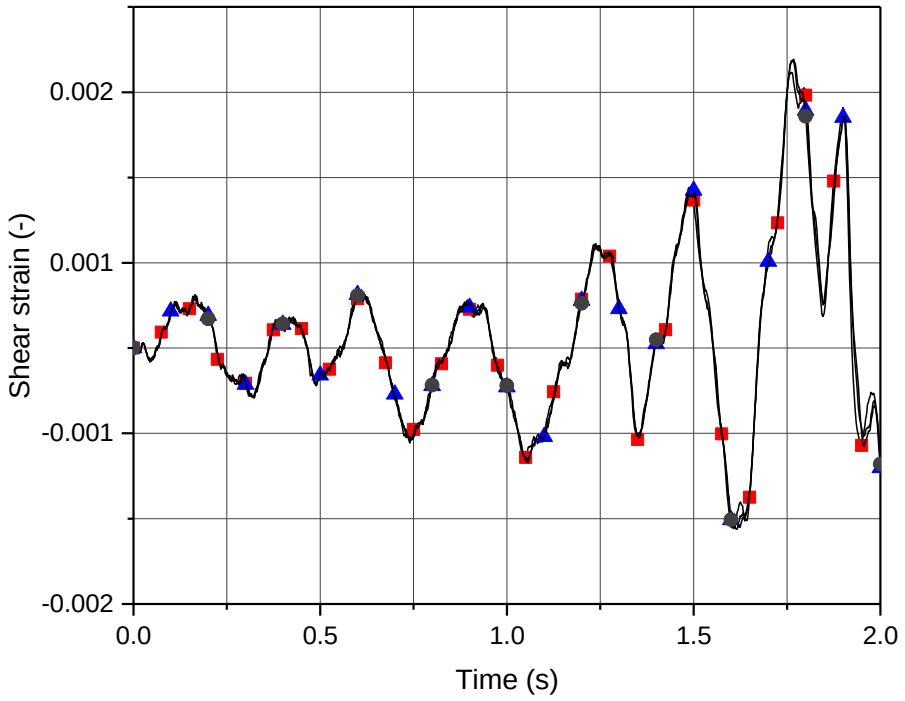

Figure 9. Shear strain convergence for ANCF24 element (25 elements, 35 elements, 45 elements)

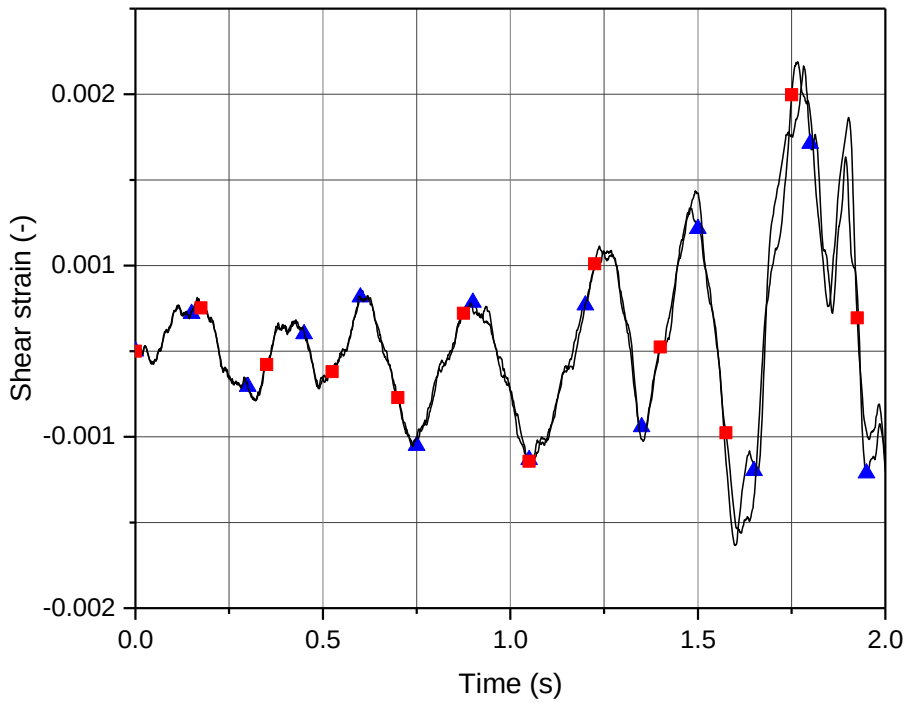

Figure 10. Shear strain comparison between ANCF24 and ANCF/CRBF18 elements (35 ANCF24 elements, 45 ANCF/CRBF18 elements)

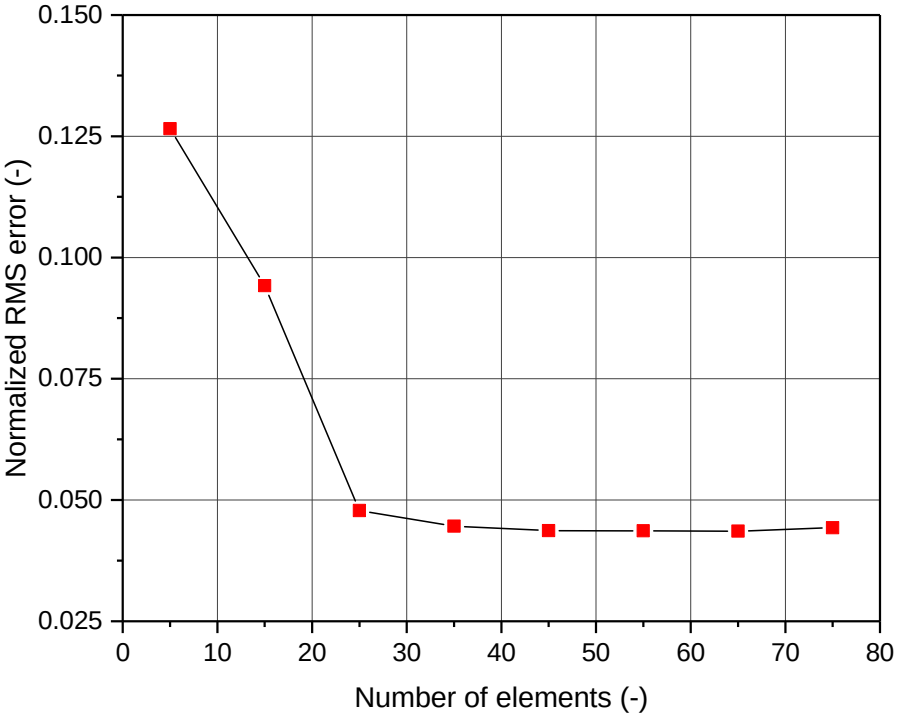

Figure 11. Shear strain normalized RMS error for ANCF/CRBF18 element

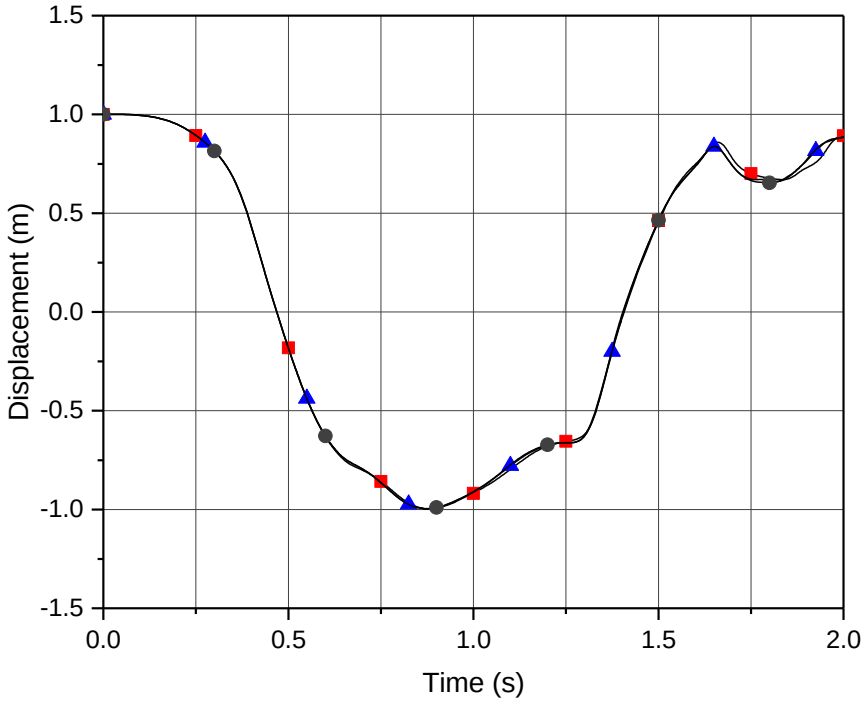

Figure 12. Pendulum tip X -displacement comparison for linear elements (—■—25 ANCF24 elements, —▲—95 LINBEAM18 elements, —●—95 CRBF12 elements)

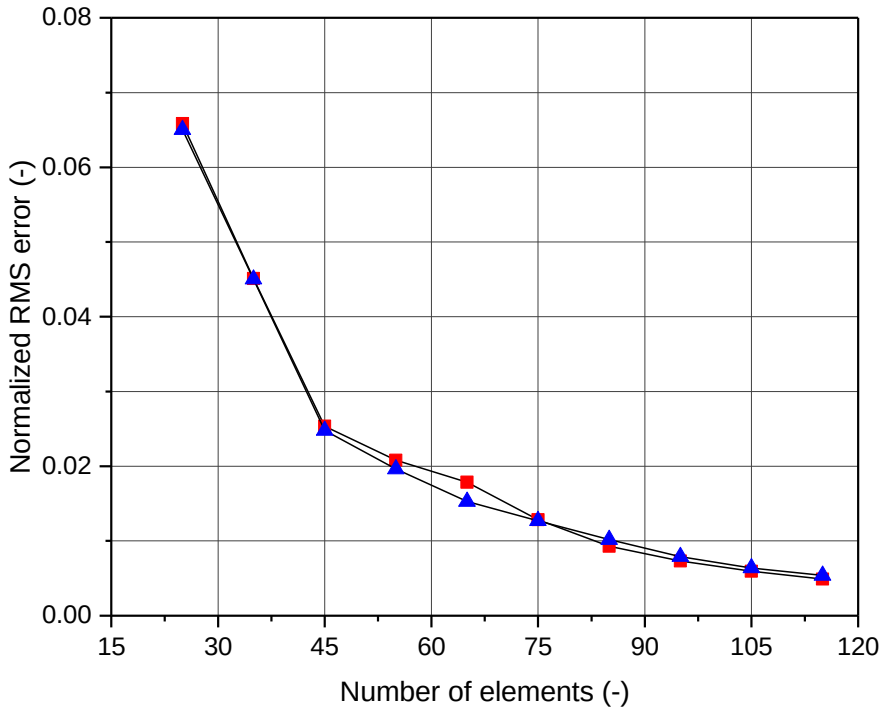

Figure 13. Tip X -displacement normalized RMS error for lower order linear elements (—■—LINBEAM18 element, —▲—CRBF12 element)

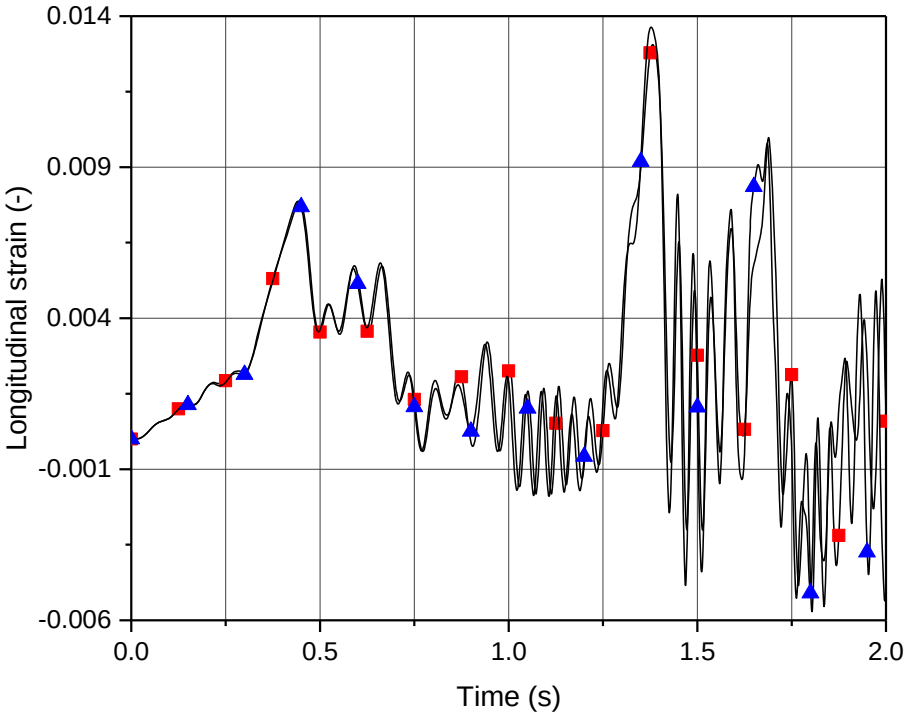

Figure 14. Longitudinal strain comparison between ANCF24 and LINBEAM18 elements

(25 ANCF24 elements, 115 LINBEAM18 elements)

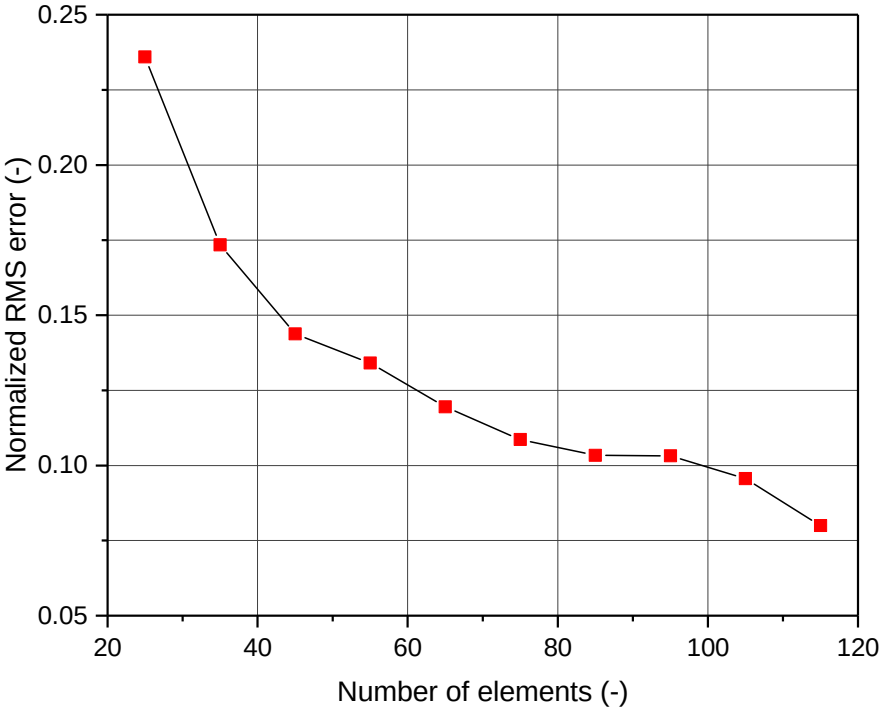

Figure 15. Longitudinal strain normalized RMS error for LINBEAM18 element

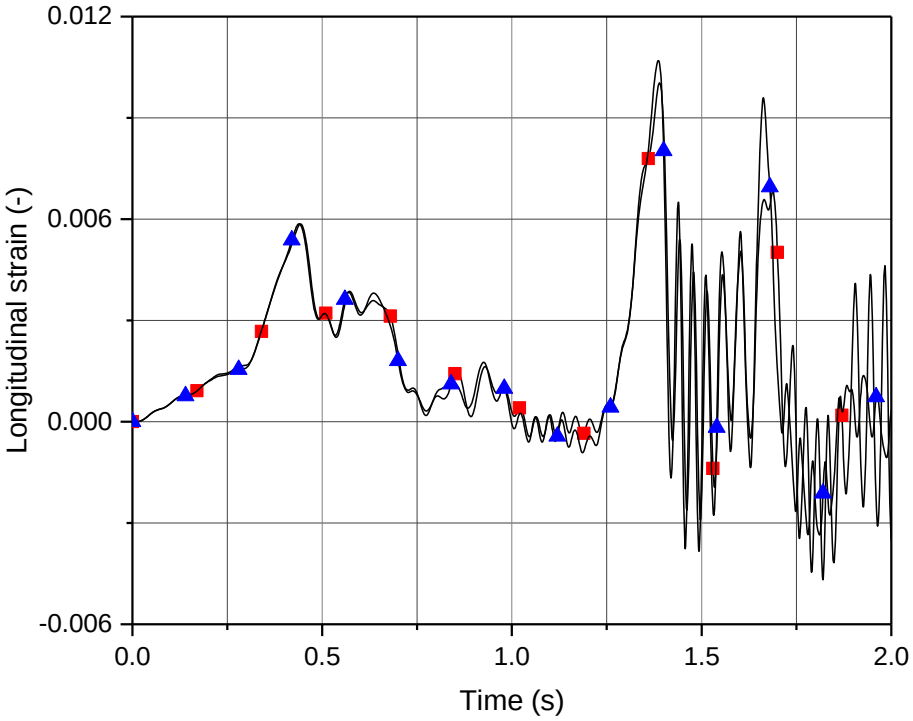

Figure 16. Longitudinal strain comparison between ANCF/CRBF18 and CRBF12 elements

(55 ANCF/CRBF18 elements, 115 CRBF12 elements)

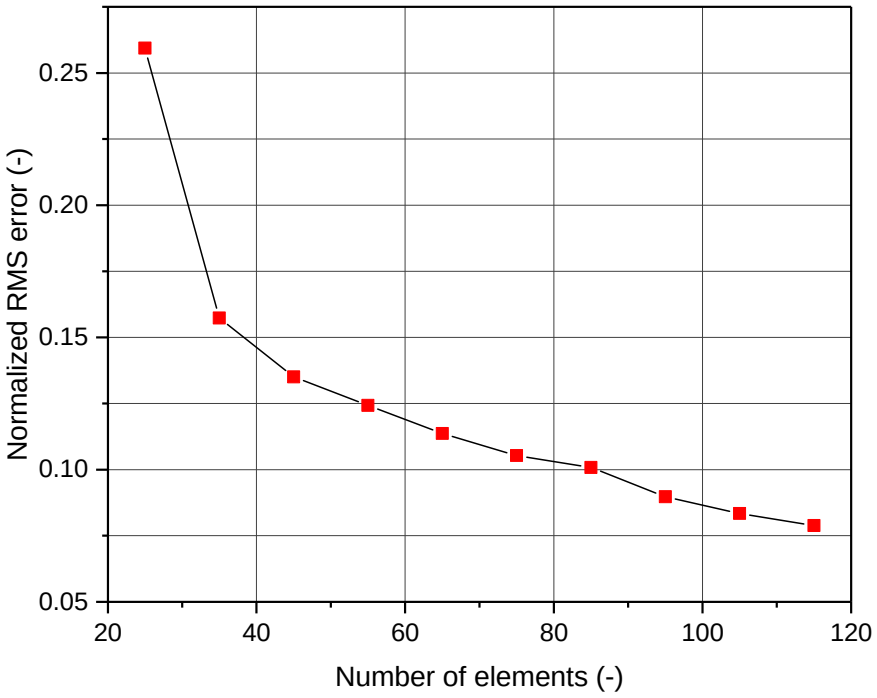

Figure 17. Longitudinal strain normalized RMS error for CRBF12 element